

Processing quantum signals carried by electrical currents

B. Roussel^{1,2}, C. Cabart¹, G. Fève³, and P. Degiovanni¹
(1) *Univ Lyon, ENS de Lyon, Université Claude Bernard Lyon 1, CNRS, Laboratoire de Physique, F-69342 Lyon, France*
(2) *European Space Agency - Advanced Concepts Team, ESTEC, Keplerlaan 1, 2201 AZ Noordwijk, The Netherlands. and*
(3) *Laboratoire de Physique de l'École Normale Supérieure, ENS, Université PSL, CNRS, Sorbonne Université, Université Paris-Diderot, Sorbonne Paris Cité, Paris, France*

Recent developments in the coherent manipulation of electrons in ballistic conductors include the generation of time-periodic electrical currents involving one to few electronic excitations per period. However, using individual electrons as carrier of quantum information for flying qubit computation or quantum metrology applications calls for a general method to unravel the single-particle excitations embedded in a quantum electrical current and how quantum information is encoded within it. Here, we propose a general signal processing algorithm to extract the elementary single-particle states, called electronic atoms of signal, present in any periodic quantum electrical current. These excitations and their mutual quantum coherence describe the excess single-electron coherence in the same way musical notes and score describe a sound signal emitted by a music instrument. This method, which is the first step towards the development of signal processing of quantum electrical currents is illustrated by assessing the quality of experimentally relevant single electron sources. The example of randomized quantum electrical currents obtained by regularly clocked but randomly injected unit charge Lorentzian voltage pulses enables us to discuss how interplay of the coherence of the applied voltage and of the Pauli principle alter the quantum coherence between the emitted single particle excitations.

Version of February 2, 2022

PACS numbers: 73.23.-b, 73.43.-f, 71.10.Pm, 73.43.Lp

Keywords: quantum physics, quantum information, signal processing, electron quantum optics, quantum Hall effect

I. INTRODUCTION

These recent years have seen spectacular breakthrough in the manipulation of quantum electric circuits. On-demand single-electron sources in quantum Hall edge channels [1–4], 2D electron gases using electron pumps [5] or surface acoustic waves [6] and in tunnel junctions [7] enable us to engineer time-dependent quantum electrical currents involving one to a few elementary excitations per period. This emerging field, called electron quantum optics, precisely aims at generating, manipulating and characterizing such “quantum beams of electricity” in metallic quantum conductors [8]. The latest advances have given access to the single-particle wavefunctions carried by such quantum electrical currents together with their emission probabilities and coherences [9] thereby demonstrating our ability to access electronic quantum states at an unprecedented level. These achievements strongly suggest that this field is now sufficiently mature for exploring its applications.

From a quantum technology point of view, quantum electrical currents carry quantum information through their single-, two- and ultimately, many-particle content. For example, single electrons delocalized on two one-dimensional channels have been proposed as “railroad flying qubit” [10–14] in which a qubit state is encoded in the quantum delocalization of an electron on two co-

propagating 1D channels [15]. This is a very promising line of research towards the development of quantum spintronics [16, 17] and, in the longer term, of free electron quantum computation [18–20].

This information can be accessed through a hierarchy of electronic coherences similar to the ones introduced by Glauber [21] for photons. These coherences are the “quantum signals” carried by the quantum electrical current in a metallic conductor. Because of the parity super-selection rule [22–24], the first non-zero electronic quantum signal is the single-electron coherence [25, 26] containing all information on single-particle excitations within the system. The next one is the second order electronic coherence [27, 28] that describes two-particle excitations within the beam.

Measuring these quantum signals requires quantum tomography protocols for n -electron coherence. Such tomography protocols are all based on the transformation of quantum signals into measurable quantities. For example, Mach-Zehnder, Hong-Ou-Mandel (HOM) and Franck electron interferometry experiments realize “filtering” or “overlaps” on electronic coherences [29], thereby encoding the results of these operations into experimentally accessible quantities such as average current [30] and current correlations [31, 32]. Electronic HOM interferometry [33] is at the core of the recently demonstrated HOM single-electron tomography [9, 34] whereas, for

higher-energy (meV) electrons, a time-dependent quantum point contact was used as a time-dependent energy filter for reconstructing single-electron coherence [35].

This however leaves open the question of decoding classical or quantum information encoded within quantum electrical currents. This requires finding appropriate representations of electronic coherences. In the present context, “appropriate” means simple with respect to the reference state which is a Fermi sea at a given chemical potential. We therefore consider the excess single-particle coherence describing the single-particle content in terms of electron and hole excitations with respect to the reference Fermi sea. Ideally, we are looking for the simplest possible description, requiring minimal data to encode this description of the single-particle content.

In this paper, we show in full generality that such a description exists: any excess time-periodic single-electron coherence admits a minimal description in terms of quasi-periodic single-electron and single-hole excitations which are the time-domain counterparts of Bloch waves in solid state physics [36]. This implies that only electron and hole Bloch wave emission probabilities as well as electron/hole coherences between two different Bloch waves are required to know the single electron coherence. Considering the counterpart of Wannier functions [37], which are localized wave-functions contrary to Bloch waves, the excess single-electron coherence can then be expressed in terms of a set of mutually orthogonal single-particle states called electronic atoms of signal [29] thereby providing us with a discrete description of the electronic coherence. We shall see that electronic atoms of signals and the discrete representation of single-electron coherence can be viewed as the counterpart of music notes and of a musical score as pictured on Fig. 1. Therefore, the extraction of such a simple form of single-electron coherence provides us with the appropriate toolbox to develop a full wave-packet based approach on quantum transport envisioned in pioneering works [38, 39]. In a broader perspective, it is a crucial step in the development of “quantum signal processing” for quantum electrical currents that extends the general paradigm of signal processing [40] to the quantum realm. It would entitle us with an enabling set of technologies and methods aiming at encoding, transferring and retrieving quantum information carried by these “quantum signals”, a crucial step for the applications of electron-based quantum technologies.

Whenever interactions can be neglected, this description can be used to describe the full many-body state of the electron fluid and therefore to access many-particle quantities such as the electron/hole entanglement entropies. This connexion can be made explicit using time periodic single scattering theory and has been used to obtain the full counting statistics of single particle excitations [41].

The entanglement entropy inferred from this representation of single-electron coherence can then be used to assess the quality of experimentally relevant single elec-

tron sources such as the mesoscopic capacitor. We are also able to obtain an explicit description of the single-electron excitations emitted. Finally, in order to illustrate the possibility for modulating emission probabilities and coherences, we apply our algorithm to the recently introduced randomized trains of Lorentzian pulses [42], an interesting example that enlightens the role of the Pauli exclusion principle in electronic quantum signals.

This paper is structured as follows: in Section II, we introduce the problem of finding a simple representation of single-electron coherence. Then, in Section III, we present our algorithm for finding such a representation for any time-periodic excess single-electron coherence. The relation of this representation to electron/hole entanglement is discussed in Section IV. Finally, we apply our method to the study of the mesoscopic capacitor to assess its quality as a single-electron source, and to periodic and randomized Leviton trains in Section V.

II. STATEMENT OF THE PROBLEM

Let us now introduce and motivate the problem considered here by considering simple trains of excitations used to model the emission by experimentally demonstrated single to few electron sources. These simple examples will enable us to write down a simple representation of the excess single-electron coherence, a generalization of which will be shown to exist in Section III.

A. Electronic coherence

The central concept of electron quantum optics are the electronic coherences defined by analogy with Glauber’s coherences of photon quantum optics [21]. They carry all the information on the fermionic n -particle states propagating within the conductor. Here we focus on single-electron coherence, which, at position x along a single chiral electronic channel, is defined as [25, 43]

$$\mathcal{G}_{\rho,x}^{(e)}(t|t') = \text{tr}(\psi(x,t) \rho \psi^\dagger(x,t')). \quad (1)$$

where ρ denotes the many-body reduced density operator for the electron fluid and ψ the fermionic field operator describing the electrons. When all the electronic sources are switched off, $\mathcal{G}_{x,\text{off}}^{(e)}$ coincides with the equilibrium single-electron coherence characterized by a chemical potential μ and an electronic temperature T_{el} . When sources are switched on, the excess single-electron coherence defined by $\mathcal{G}_{x,\text{on}}^{(e)} = \mathcal{G}_{x,\text{off}}^{(e)} + \Delta\mathcal{G}_x^{(e)}$ contain all the information on the single-particle excitations generated by the sources and drives that are switched on.

The single-electron coherence can be studied in the time domain as well as in the frequency domain but is most conveniently visualized using a real-valued time/frequency representation called the Wigner distri-

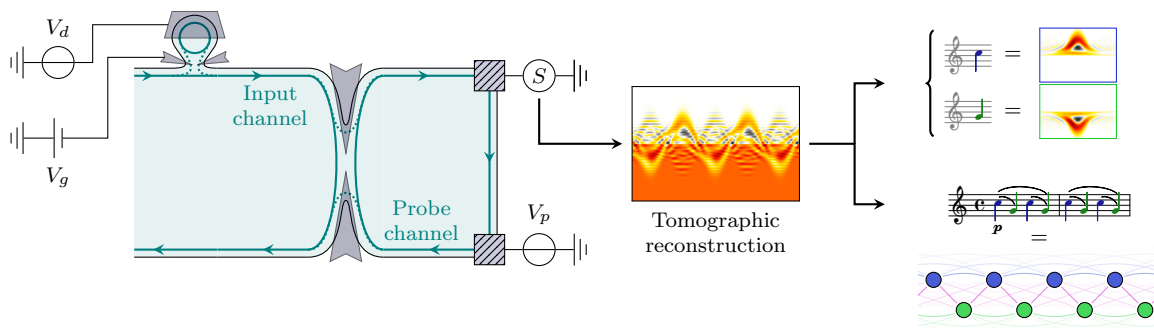


FIG. 1: Schematic of the process for extracting the single particle content from a quantum electrical current. Left part: the Hong–Ou–Mandel interferometer uses two-particle interferences to encode the overlap between the injected single electron coherences into the outgoing current noise [29]. Middle part: the single electron coherence is reconstructed from current noise measurements [34, 43, 44]. Right part: the result of the tomographic reconstruction, depicted here as the electronic Wigner distribution function [45], is processed by the algorithm described in the present paper to obtain a description of single electron coherence in terms of electronic atoms of signal (counterparts of musical notes) arranged according to a “quantum coherence score” (counterpart of the music score).

bution function [45]

$$W_{\rho,x}^{(e)}(t, \omega) = \int_{\mathbb{R}} v_F \mathcal{G}_{\rho,x}^{(e)} \left(t + \frac{\tau}{2} \middle| t - \frac{\tau}{2} \right) e^{i\omega\tau} d\tau \quad (2)$$

B. Electron and hole trains

An ideal periodic single-electron source is a periodically operated device that emits exactly one single-electron excitation on top of the Fermi sea $|F_{\mu=0}\rangle$ during each period. The corresponding many body state is an electron train of the form

$$|\Psi_{\text{SES}}\rangle = \prod_{l \in \mathbb{Z}} \psi^\dagger[\varphi_{e,l}] |F_{\mu=0}\rangle \quad (3)$$

where $\psi^\dagger[\varphi_{e,l}]$ creates a single particle excitation in the electronic wavefunction $\varphi_{e,l}$. It differs from $\varphi_{e,l=0}$ by translation by lT in the time domain. Ideally, one would like each of these electronic excitations to be perfectly distinguishable from each other which means that $\varphi_{e,l}$ and $\varphi_{e,l'}$ are orthogonal when $l \neq l'$. In this case, the excess single-electron coherence is

$$\Delta \mathcal{G}^{(e)}(t|t') = \sum_{l=-\infty}^{+\infty} \varphi_{e,l}(t) \varphi_{e,l}(t')^* \quad (4)$$

For example, when driven by a square gate voltage $V_g(t)$ and for a suitable value of the dot transparency $D = D_{\text{opt}}$ the mesoscopic capacitor depicted on Fig. 2 ideally generates one electron excitation and one hole excitation per period [1, 46]:

$$|\Psi_{\text{MC-SES}}\rangle = \prod_{l=-\infty}^{+\infty} \psi^\dagger[\varphi_{e,l}] \psi[\varphi_{h,l}] |F_{\mu=0}\rangle \quad (5)$$

Here $\varphi_{e,l}$ and $\varphi_{h,l}$ are time translated by lT from the emitted electron $\varphi_{e,0}$ and hole wavefunctions $\varphi_{h,0}$ and are mutually orthogonal and normalized. The excess single-electron coherence is then given by

$$\Delta \mathcal{G}^{(e)} = \sum_{l=-\infty}^{+\infty} \varphi_{e,l}(t) \varphi_{e,l}(t')^* - \sum_{l=-\infty}^{+\infty} \varphi_{h,l}(t) \varphi_{h,l}(t')^* \quad (6)$$

where the hole contribution naturally comes with a minus sign.

When closing the dot, the time needed to emit an electronic (or hole) excitation becomes larger than $T/2$. It was then argued [43] that the mesoscopic capacitor emits a quantum superposition of no excitation and an elementary electron/hole pair during each period. Such a state would be parametrized as

$$|\Psi_{e/h}(u, v)\rangle = \prod_{l=-\infty}^{+\infty} (u + v\psi^\dagger[\varphi_{e,l}]\psi[\varphi_{h,l}]) |F_{\mu=0}\rangle \quad (7)$$

where $|u|^2 + |v|^2 = 1$. The resulting single-electron coherence is then

$$\Delta \mathcal{G}^{(e)}(t|t') = \sum_{l \in \mathbb{Z}} [|v|^2 \varphi_{e,l}(t) \varphi_{e,l}(t')^* - |v|^2 \varphi_{h,l}(t) \varphi_{h,l}(t')^*] \quad (8a)$$

$$+ \sum_{l \in \mathbb{Z}} [u v^* \varphi_{e,l}(t) \varphi_{h,l}(t')^* + v u^* \varphi_{h,l}(t) \varphi_{e,l}(t')^*] \quad (8b)$$

in which the r.h.s. of Eq. (8a) lives in the quadrants of electron and hole excitations (see Fig. 3) whereas Eq. (8b) represents the electron/hole pair coherence arising from $|\Psi_{e/h}(u, v)\rangle$ whenever $uv \neq 0$. Equation (6) is recovered

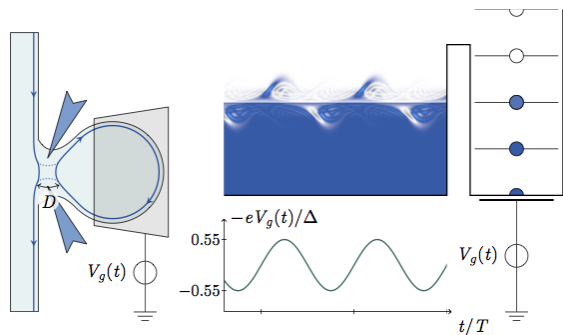


FIG. 2: Left panel: The mesoscopic capacitor is a ballistic quantum conductor formed by connecting a quantum dot to a chiral edge channel via a quantum point contact of transparency D . Right panel: Modelization as a driven quantum dot with level spacing Δ connected to an electronic reservoir. The mesoscopic capacitor is driven by an a.c. voltage drive $V_g(t)$ applied to the top gate. Applying a d.c. voltage bias to the top gate shifts the energy levels of the dot. The mesoscopic capacitor emits a stream of electron and hole excitations whose Wigner distribution function $W_S^{(e)}(t, \omega)$ is depicted as a density plot on the right panel.

for $(u, v) = (0, 1)$ which should therefore correspond to $D \simeq D_{\text{opt}}$ whereas for $(u, v) = (1, 0)$ one recovers the Fermi sea, the result expected when the dot is totally closed ($D = 0$). The case where $|u|^2 = |v|^2 \simeq 1/2$ could thus be viewed as the excess electronic coherence from an ideal source emitting a coherent superposition of “nothing” and of a single electron/hole pair per period. It corresponds to maximal electron/hole entanglement [29]. Note however that the r.h.s of Eq. (8) does not involve inter-period coherences (terms with $l \neq l'$).

C. Electronic atoms of signal

Equations (4), (6) and (8) correspond to ideal sources and have a simple expression in terms of a family of single-electron wavefunctions called *electronic atoms of signal* [29]. Electronic atoms of signal consists in a family of normalized mutually orthogonal single-electron wavefunctions $\varphi_{a,l}$ which are translated by multiples of T :

$$\varphi_{a,l}(t) = \varphi_{a,0}(t - lT) \quad (9a)$$

$$\langle \varphi_{a,l} | \varphi_{a',l'} \rangle = \delta_{l,l'} \delta_{a,a'}. \quad (9b)$$

Although a decomposition of the form (4) is known [47] for a T -periodic train of Lorentzian voltages pulses of unit charge at zero temperature, realistic sources are, in general, not ideal. Even the forms given by expressions (6) and (8) are too simple to describe the excess single-electron coherence of all experimentally realistic sources. First of all, even at very low temperature, they correspond to ideal operating regimes which are only asymptotic with respect to the experimental parameters as in

the case of the mesoscopic capacitor at $D \simeq D_{\text{opt}}$. Moreover, at non-zero temperature T_{el} , electron/hole pairs are generated from thermal fluctuations and introduce an underlying thermal coherence time $\hbar/k_B T_{\text{el}}$ a priori unrelated to the period T . It may lead to interperiod coherences not present in expression 8. Last but not least, when electronic coherence is measured at some distance from such a source, Coulomb interactions alter the electronic coherence in a drastic way [48–50], leading to extra-electron/hole pairs [51].

These remarks rise the question of finding a way to express an arbitrary periodic single-electron coherence in terms of suitable electronic atoms of signals. We will now present a systematic procedure for obtaining such an expression together with the appropriate electronic atoms of signals from single-electron coherence. This procedure can be applied to data obtained from a numerical computation but also to experimental data obtained from an electronic tomography protocol as recently demonstrated in [9].

III. FLOQUET–BLOCH–WANNIER ANALYSIS

A. Sketch of the method

Equations (4), (6) and (8) have in common that their purely electron and purely hole parts are very simple. This characteristic is at the heart of our signal processing algorithm for analyzing single-electron coherence. The key idea, which is to exploit time periodicity of single-electron coherence

$$\mathcal{G}_{\rho,x}^{(e)}(t + T | t' + T) = \mathcal{G}_{\rho,x}^{(e)}(t | t'), \quad (10)$$

lies at the heart of Floquet theorem [52], the time-domain counterpart of Bloch’s theorem for electronic waves in a periodic crystal [36].

However, in the present situation, we are looking for a simple description of $\mathcal{G}_{\rho}^{(e)}$ in terms of electron and hole excitations with respect to a reference Fermi sea (here $|F_{\mu=0}\rangle$). Consequently, Floquet’s theorem has to be adapted in order to be compatible with the decomposition of the single-particle space of states into a direct sum $\mathcal{H} = \mathcal{H}_+ \oplus \mathcal{H}_-$ of electron and hole excitations that have positive (resp. negative) energy with respect to the $\mu = 0$ Fermi level. As we shall see, this can be done and the corresponding eigenvalues have a transparent physical meaning as an occupation number. Finally, as in band theory of solids, localized single-particle states [37] can then be constructed. We will show in Section III C that these are the electronic atoms of signals suitable for describing the quantum electrical current under consideration.

B. Floquet–Bloch analysis

Introducing localized single-particle states $|t\rangle$ such that $\langle t|t'\rangle = v_F^{-1}\delta(t-t')$, the dimensionless Hermitian operator $\mathbf{G}^{(e)}$ is defined by

$$\mathbf{G}^{(e)} = v_F^2 \int_{\mathbb{R}^2} |t\rangle \mathcal{G}^{(e)}(t, t') \langle t'| dt dt'. \quad (11)$$

in which the (ρ, x) index has been dropped out for simplicity. The conjugation relation $\mathcal{G}^{(e)}(t|t')^* = \mathcal{G}^{(e)}(t'|t)$ for single-electron coherence translates into $\mathbf{G}^{(e)}$ being Hermitian. Furthermore, if we introduce the single-particle state $|\varphi\rangle$ corresponding to an excitation described by a normalized wavefunction φ

$$|\varphi\rangle = v_F \int_{\mathbb{R}} \varphi(t) |t\rangle dt, \quad (12)$$

its occupation probability is a real number between 0 and 1 given by

$$p[\varphi] = \langle \varphi | \mathbf{G}^{(e)} | \varphi \rangle. \quad (13)$$

thereby ensuring that $\mathbf{G}^{(e)}$ is a positive operator, bounded by 1. For a T -periodic source, time periodicity of single-electron coherence translates into the commutation of $\mathbf{G}^{(e)}$ with the time-translation operator \mathbf{T}_T defined by $\mathbf{T}_T|t\rangle = |t+T\rangle$.

As explained before, our analysis has to be performed separately on the electron and hole subspaces \mathcal{H}_{\pm} . The

adapted Floquet-Bloch theorem proven in Appendix B provides us with a basis of single-particle state which partially diagonalizes the single-electron operator while being compatible with the decomposition into electron and hole excitations.

More precisely, this result states that there exists an orthonormal basis $|\psi_{a,\nu}^{(e)}\rangle$ of the positive-energy Hilbert space \mathcal{H}_+ and an orthonormal basis $|\psi_{b,\nu}^{(h)}\rangle$ of the negative-energy Hilbert space \mathcal{H}_- which are respectively indexed by band indexes a (resp. b) and quasi-energies $0 \leq \nu < 2\pi f$ which are all eigenvectors of the time-translation operator \mathbf{T}_T with eigenvalue $e^{-i\nu T}$ and satisfy the normalization condition

$$\langle \psi_{a,\nu}^{(e)} | \psi_{a',\nu'}^{(e)} \rangle = 2\pi \delta_{a,a'} \delta_{\mathbb{R}/2\pi f\mathbb{Z}}(\nu - \nu'). \quad (14)$$

where $\delta_{\mathbb{R}/2\pi f\mathbb{Z}}$ is a Dirac comb of period $2\pi f$. A similar relation is obtained for the hole states $|\psi_{b,\nu}^{(h)}\rangle$. In this basis, the projections of the single-electron operators on the electron and hole quadrants (see Fig. 3) are diagonalized and their eigenvalues can be expressed as the occupation numbers of the corresponding single-electron states. Finally, the full electronic coherence $\mathbf{G}^{(e)}$ also contains the information on electron/hole coherences (see Fig. 3) which also commutes with \mathbf{T}_T . As explained in Appendix B, all this leads to the following form of single-electron coherence:

$$\mathbf{G}^{(e)} = \int_0^{2\pi f} \left(\sum_a g_a^{(e)}(\nu) |\psi_{a,\nu}^{(e)}\rangle \langle \psi_{a,\nu}^{(e)}| + \sum_b (1 - g_b^{(h)}(\nu)) |\psi_{b,\nu}^{(h)}\rangle \langle \psi_{b,\nu}^{(h)}| \right) \frac{d\nu}{2\pi} \quad (15a)$$

$$+ \sum_{a,b} \int_0^{2\pi f} \left(g_{ab}^{(eh)}(\nu) |\psi_{a,\nu}^{(e)}\rangle \langle \psi_{b,\nu}^{(h)}| + g_{ba}^{(he)}(\nu) |\psi_{a,\nu}^{(e)}\rangle \langle \psi_{b,\nu}^{(h)}| \right) \frac{d\nu}{2\pi}, \quad (15b)$$

where $g_{ab}^{(eh)}(\nu) = g_{ba}^{(he)}(\nu)^*$ in order to ensure hermiticity of $\mathbf{G}^{(e)}$. Let us note that the Floquet-Bloch wavefunctions being quasi-periodic, these are extended states which are not localized on a specific period. This is not yet the description in terms of electronic atoms of signals that will be discussed in the forthcoming subsection. Before moving to this description, let us recall that the outcome of the electronic tomography protocol originally proposed in Ref. [43] is an experimental determination of $\Delta_0 \mathbf{G}^{(e)}$ to which the diagonalization procedure can be applied, therefore leading to an Floquet-Bloch electronic and hole eigenstates and spectrum as was done in [9].

As discussed in Appendix B, the restriction $\mathbf{G}_{++}^{(e)}$ of the coherence operator $\mathbf{G}^{(e)}$ to the electron quadrant, is also

positive and bounded by 1. This leads to $0 \leq g_a^{(e)}(\nu) \leq 1$ for all (a, ν) , thus showing that they can be interpreted as the occupation number for the Floquet-Bloch electronic states $|\psi_{a,\nu}^{(e)}\rangle$. In the same way, $0 \leq g_b^{(h)}(\nu) \leq 1$ since $1 - g_b^{(h)}(\nu)$ is the occupation number of the hole electronic state $|\psi_{b,\nu}^{(h)}\rangle$.

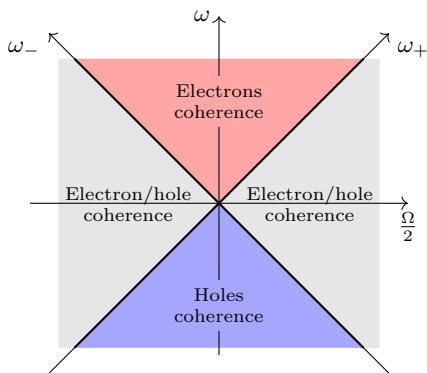


FIG. 3: Frequency domain quadrants for single-electron coherence: depending on the signs $(\varepsilon_+, \varepsilon_-)$ of (ω_+, ω_-) , we are considering the matrix elements $\langle \omega_- | \mathbf{G}^{(e)} | \omega_+ \rangle$ of $\mathbf{G}_{\varepsilon_+, \varepsilon_-}^{(e)}$ in the $|\omega\rangle$ basis of plane waves (see Appendix A for normalizations). The electronic quadrant (in red) defined by both $\omega_+ = \omega + \Omega/2$ and $\omega_- = \omega - \Omega/2$ positive gives information about electronic excitations. The hole quadrant (in blue) defined by both ω_+ and ω_- being negative gives information about hole excitations. The two electron/hole quadrants ($\omega_+ \omega_- < 0$, light grey) contain information about electron/hole coherences.

C. Electronic atoms of signal

1. Floquet-Wannier states

Since we are interested into finding a description of the excess single-electron coherence in terms of electronic atoms of signal [29] which are normalized localized single-electron states, we consider Floquet-Wannier states which are the analogous of localized orbitals in solid-state band theory [37]. They are defined for $l \in \mathbb{Z}$ as

$$|\varphi_{a,l}\rangle = \frac{1}{\sqrt{f}} \int_0^{2\pi f} e^{-i\nu l t} |\psi_{a,\nu}\rangle \frac{d\nu}{2\pi}, \quad (16)$$

and form an orthonormal family as implied by Eq. (14). Moreover, for a given band, all the states $(|\varphi_{a,l}\rangle)_{l \in \mathbb{Z}}$ are related by time translation since $\mathbf{T}_T |\psi_{a,\nu}\rangle = e^{-i\nu T} |\psi_{a,\nu}\rangle$ and Eq. (16) imply that:

$$\mathbf{T}_T |\varphi_{a,l}\rangle = |\varphi_{a,l+1}\rangle. \quad (17)$$

Exactly as in solid-state band theory [53], there are ambiguities in the determination of electronic atoms of signals coming from the possibility to redefine the Floquet-Bloch eigenvectors at a given quasi-energy ν within each degenerate subspace of the projection of $\mathbf{G}^{(e)}$ on the electron or the hole subspace. These ambiguities are extensively discussed in Appendix C. To circumvent these difficulties, we will focus here on the electronic atoms of signal that have the smallest spreading in time. This minimal spreading principle [53], detailed in Appendix C 2, has the advantage of producing maximally localized electronic atoms of signal. This provides a clear view of

single-electron coherence within the electronic fluids in terms of single-particle states that are most visibly associated with a given period.

To understand the meaning of such a description, a musical analogy is convenient: the sound signal associated with a music instrument can be described in terms of elementary units which are “music notes” arranged along a “music score” which specifies the notes to be emitted at a given time. The electronic atoms of signal can indeed be viewed as the electron quantum optics counterparts of “notes” and the expression of the excess single-electron coherence in the basis of “notes” can be viewed as its “quantum coherence score”. We will now discuss the specific form of the “quantum coherence score” of a T -periodic single electron coherence.

2. Quantum coherence score

The single-electron coherence restricted to the electronic quadrant $\mathbf{G}_{++}^{(e)}$ can then be rewritten as

$$\mathbf{G}_{++}^{(e)} = \sum_a \sum_{l_+, l_-} g_a^{(e)}(l_+ - l_-) |\varphi_{a,l_+}\rangle \langle \varphi_{a,l_-}| \quad (18)$$

where

$$g_a^{(e)}(l) = \int_0^{2\pi f} g_a^{(e)}(\nu) e^{i\nu T l} \frac{d\nu}{2\pi f}. \quad (19)$$

For $l \neq 0$, $g^{(e)}(l)$ represents the interperiod coherence over $|l|$ periods whereas $g_a^{(e)}(0)$ is the emission probability for the φ_a electronic atom of signal at each period. Note that there is no coherence between electronic atoms of signals associated with different bands. However, electronic coherence may extend over more than one time period: a flat band ($g_a^{(e)}(\nu)$ constant) won't lead to inter-period coherences whereas a non-flat band will. The typical scale over which $g_a^{(e)}(\nu)$ varies is nothing but the inverse timescale over which inter-period coherence exists. The same considerations apply to hole bands. Finally, using these Floquet-Wannier states, the electron/hole coherences $g_{ab}^{(eh)}(l_+ - l_-) = \langle \varphi_{b,l_-}^{(h)} | \mathbf{G}^{(e)} | \varphi_{a,l_+}^{(e)} \rangle$ in this basis are given by

$$g_{ab}^{(eh)}(l) = \int_0^{2\pi f} g_{ab}^{(eh)}(\nu) e^{i\nu T l} \frac{d\nu}{2\pi f}. \quad (20)$$

Because electron/hole coherence couples different bands, different choices of electronic atoms of signal lead to different values for $g_{ab}^{(eh)}(\Delta l)$. This is not the case for the coherence between purely electronic or purely hole wavepackets given by Eq. (19).

Note that inter-period and electron/hole coherences make the “quantum coherence score” richer than an ordinary (classical) music score which only specifies the note that has to be played at a given time and its intensity.

The electronic atoms of signal and the associated “quantum coherence score” are the natural language to describe an arbitrary excess single-electron coherence. The “quantum coherence score” could in principle be used to encode some quantum information within a quantum electrical current.

Exactly as a tight-binding quadratic Hamiltonian in a specific Wannier orbital basis is a natural way to describe electron hopping within a condensed-matter system, the “quantum coherence score” is the first step in characterizing the many-body state of the electronic system. The excess second-order electronic coherence [28] can also be expressed in terms of electronic atoms of signal, thereby providing a view of the first non-trivial electronic correlations within the electronic fluid. Understanding the many-body state of the electronic fluid in terms of these discrete representations of first- and higher-order excess electronic coherences is a very interesting perspective for electron quantum optics. Although its simplest aspect will be discussed in Section IV, a full discussion would go way beyond the scope of the present paper.

Positivity of the electronic and hole coherences $\mathbf{G}^{(e)}$ and $\mathbf{G}^{(h)}$ leads to Cauchy-Schwarz inequalities. Within the electron and hole quadrants, it leads to

$$\left| g_a^{(e)}(l) \right| \leq \min(g_a^{(e)}, 1 - g_a^{(e)}) \quad (21a)$$

$$\left| g_b^{(h)}(l) \right| \leq \min(g_b^{(h)}, 1 - g_b^{(h)}) \quad (21b)$$

with $g_a^{(e)} = g_a^{(e)}(l=0)$ and $g_b^{(h)} = g_b^{(h)}(l=0)$ denoting the respective averages of $g_a^{(e)}(\nu)$ and $g_b^{(h)}(\nu)$ over $0 \leq \nu < 2\pi f$. In the electron/hole quadrants, the Cauchy-Schwarz inequalities bound the electron/hole coherences:

$$\left| g_{ab}^{(eh)}(l) \right|^2 \leq g_a^{(e)} \left(1 - g_b^{(h)} \right) \quad (22a)$$

$$\left| g_{ab}^{(eh)}(l) \right|^2 \leq g_b^{(h)} \left(1 - g_a^{(e)} \right). \quad (22b)$$

These inequalities immediately show that, in the absence of electron ($g_a^{(e)}(\nu) = 0$ for all ν and a) or hole ($g_b^{(h)}(\nu) = 0$) excitations, there are no electron/hole coherences ($g_{ab}^{(eh)}(l) = 0$) as well as no coherence between the missing excitations as noted in Ref. [45].

3. Martin-Landauer wavepackets

Let us illustrate these ideas on the example of a stationary electronic state. In this case, the single-electron coherence only depends on $t - t'$ and is the Fourier transform of the electronic distribution function $f_e(\omega)$. Such a state can be viewed as T -periodic for any period T so, let us choose one and perform the corresponding Floquet–Bloch analysis. The excess single-electron coherence being already diagonal in the plane-wave basis, the Floquet–Bloch waves are plane waves $\psi_{m,\nu}(t) =$

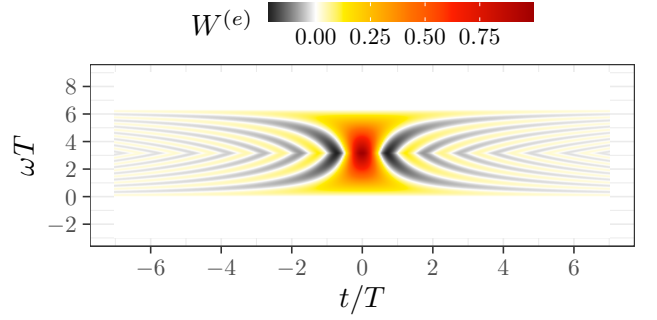


FIG. 4: Wigner representation of the Martin-Landauer wavepacket $ML_{0,0}$ as a function of t/T and ωT .

$v_F^{-1/2} e^{-i(\nu+2\pi mf)t}$ ($0 \leq \nu < 2\pi f$). The bands are then indexed by an integer $m \in \mathbb{N}$ and the corresponding eigenvalues are given by:

$$g_m^{(e)}(\nu) = f_e(\nu + 2\pi mf). \quad (23)$$

The corresponding electronic atoms of signal are obtained by summing plane waves over an energy band of width hf , centered at energies $(m + 1/2)hf$ with m integer. These are the Martin–Landauer wavepackets [38]:

$$ML_{m,0}(t) = \frac{1}{\sqrt{v_F T}} \frac{\sin(\pi ft)}{\pi ft} e^{-2i\pi(m+1/2)ft} \quad (24)$$

which are known in the signal-processing community as the Shannon wavelets. Their Wigner representation $W_{ML_{m,t}}(t, \omega) = W(t, \omega - 2\pi(m+1/2)f)$, defined for a single electron wavepacket φ by using $\varphi(t + \tau/2)\varphi(t - \tau/2)^*$ instead of $\mathcal{G}^{(e)}(t + \tau/2, t - \tau/2)$ in Eq. (2), are time and frequency translated from

$$W(t, \omega) = \Theta[\pi f - |\omega|] \left(1 - \frac{|\omega|}{\pi f} \right) \text{sinc}(2(\pi f - |\omega|)t) \quad (25)$$

The Wigner representation $W_{ML_{0,0}}$, depicted on Fig. 4, is clearly localized in the $0 \leq \omega \leq 2\pi f$ energy band and decays as $\sim 1/t$ in time.

Because of Eq. (23), the bands are generically not flat thereby implying the existence of interperiod coherences and therefore, of an associated coherence time. The idea is then to choose the period T so that, the electron distribution function is as flat as possible over energy bands of width hf .

For example, at zero temperature, the non-equilibrium distribution function generated by a d.c. biased QPC with $V_{dc} < 0$, is a step function that jumps from 1 for $\omega < 0$ to the transmission probability $0 < \mathcal{T} < 1$ from the biased incoming electrode to the outgoing one we are considering for $0 \leq \omega \leq -eV_{dc}/\hbar$. It then abruptly falls to zero $\omega > -eV_{dc}/\hbar > 0$. The natural choice of T is then $T = \hbar/e|V_{dc}|$. The excess coherence has only one non trivial band corresponding to $g_0^{(e)}(\nu) = \mathcal{T}$ for $0 \leq \nu < 2\pi f = |eV_{dc}|/\hbar$. The excess electronic coherence

is then naturally described in terms of Martin-Landauer wavepackets associated with period $T = h/e|V_{dc}|$:

$$\Delta_0 \mathbf{G}^{(e)} = \mathcal{T} \sum_{l \in \mathbb{Z}} |\text{ML}_{0,l}\rangle \langle \text{ML}_{0,l}|. \quad (26)$$

Consequently, this excess single-electron coherence corresponds to a train of Martin-Landauer wavepackets without interperiod coherences and each of them being emitted with probability \mathcal{T} . Stationarity is visible through the invariance of $\Delta_0 \mathbf{G}^{(e)}$ through translation by $\mathbf{T}_{\Delta t}$ for any Δt : timeshifting all the Martin-Landauer wavepackets in the r.h.s. of Eq. (26) $|\text{ML}_{m,l}\rangle \mapsto \mathbf{T}_{\Delta t} |\text{ML}_{m,l}\rangle$ still gives $\Delta_0 \mathbf{G}^{(e)}$.

At finite temperature $T_{\text{el}} > 0$ K, the electronic distribution function is smeared over a scale $k_B T_{\text{el}}/\hbar$, thus leading to a non-flat band spectrum. Therefore, there are always inter-period coherences over the thermal coherence time $h/k_B T_{\text{el}}$. It might seem surprising that when $T_{\text{el}} = 0$ K, the inter-period coherences go to zero whereas the thermal coherence time goes to infinity. This comes from the fact that when decreasing the temperature, as the off-diagonal coherences spread over more and more period, their modulus decreases and ultimately vanishes at zero temperature.

D. Relation to experimentally-relevant quantities

Let us now explain how experimental signals are related to these spectral quantities. We will first discuss the value of the dip in an HOM experiment, a simple HOM based repeated detection scheme of a given electronic excitation and finally a time-dependent energy filter based on a driven QPC [54].

1. The Hong–Ou–Mandel dip

In the case of an HOM experiment with two identical sources S_1 and S_2 on the incoming channels of a beam splitter with reflexion and transmission probabilities \mathcal{R} and \mathcal{T} , the depth of the HOM dip, obtained by synchronizing the sources, can be related to the Floquet-Bloch spectral properties of single-electron coherence. This comes from the expression of the two-particle interference contribution to low-frequency noise in an HOM experiment as [43]:

$$\mathcal{Q}(t, t') = -e^2 v_F^2 \mathcal{R} \mathcal{T} \left(\mathcal{G}_1^{(e)}(t, t') \mathcal{G}_2^{(h)}(t, t') + [1 \leftrightarrow 2] \right). \quad (27)$$

We consider the low frequency noise defined by integrating over $\tau = t - t'$ and averaging over $\bar{t} = (t + t')/2$. Expanding both contributions in the r.h.s. of Eq. (27) in terms of $\Delta_0 \mathbf{G}^{(e)}$ leads to three distinct contributions. Two of them involve only one of the incoming excess single-electron coherences and correspond to the partitioning of single-particle excitations from one of the

two incoming channels at the QPC (HBT contribution) whereas the third one involves the excess single electron coherence of both sources and accounts for two-particle interferences between them (HOM contribution).

At zero temperature and with identical and synchronized sources on two incoming channels the excess noise in the HBT (only one source *on*) and HOM experiments (both sources *on*) are obtained as sums of a background which comes from the transmitted or reflected excess noise ΔS_S of the sources and of two-excitation interference contributions denoted by ΔS_{HBT} and ΔS_{HOM} :

$$\Delta S_{11}^{(\text{HBT}_1)} = \mathcal{R}^2 \Delta S_S + \Delta S_{\text{HBT}} \quad (28a)$$

$$\Delta S_{11}^{(\text{HBT}_2)} = \mathcal{T}^2 \Delta S_S + \Delta S_{\text{HBT}} \quad (28b)$$

$$\Delta S_{11}^{(\text{HOM})} = (\mathcal{R}^2 + \mathcal{T}^2) \Delta S_S + \Delta S_{\text{HOM}}. \quad (28c)$$

As shown in Appendix D, ΔS_{HBT} and ΔS_{HOM} are given by:

$$\Delta S_{\text{HBT}} = e^2 \mathcal{R} \mathcal{T} \int_0^{2\pi f} \left(\sum_a g_a^{(e)}(\nu) + \sum_b g_b^{(h)}(\nu) \right) \frac{d\nu}{2\pi} \quad (29a)$$

$$\begin{aligned} \Delta S_{\text{HOM}} = & 2e^2 \mathcal{R} \mathcal{T} \left[\int_0^{2\pi f} \sum_a (1 - g_a^{(e)}(\nu)) g_a^{(e)}(\nu) \frac{d\nu}{2\pi} \right. \\ & + \int_0^{2\pi f} \sum_b g_b^{(h)}(\nu) (1 - g_b^{(h)}(\nu)) \frac{d\nu}{2\pi} \\ & \left. - 2 \int_0^{2\pi f} \sum_{a,b} |g_{ab}^{(eh)}(\nu)|^2 \frac{d\nu}{2\pi} \right]. \quad (29b) \end{aligned}$$

In Appendix D 2, we show that the depth of the HOM dip, which is the difference $\Delta S_{\text{dip}} = 2\Delta S_{\text{HBT}} - \Delta S_{\text{HOM}}$ at this operating point can be expressed simply in terms of the fluctuation of the total charge emitted per period $(\Delta Q)_w^2$:

$$\frac{[\Delta S_{\text{dip}}]}{[\Delta S_{\text{dip}}^{(\text{max})}]} = 1 - \frac{(\Delta Q)_w^2}{\bar{N}_{\text{tot}}}. \quad (30)$$

in which \bar{N}_{tot} is the sum of the average number of electron and hole excitations (see Eq. (D11)) and $(\Delta Q)_w^2$ is computed from first order coherences using Wick's theorem (see Appendix D 2). If the many-body state does satisfy Wick's theorem, which is the case whenever interactions can be neglected, then this corresponds to the actual vanishing of charge fluctuations. Under this hypothesis, an ideal single electron (see Eq. (4)) or single electron and single hole (see Eq. (6)) source would reach this bound and therefore, under the assumption that interactions can be neglected, would lead to a maximally deep HOM dip at zero temperature. Another important example is the state with a single coherent electron/hole pair obtained by the action of an operator of the form

$$\sqrt{1-g} \mathbf{1} + e^{i\Theta} \sqrt{g} \psi^\dagger [\varphi_e] \psi [\varphi_h] \quad (31)$$

where $0 < g < 1$, acting on the Fermi sea $|F_{\mu=0}\rangle$. In this case, the average number of electron (as well as hole) excitations is g but the charge fluctuation is exactly zero: $(\Delta Q)_w^2 = 0$. Consequently, the dip does to its maximum value. As we shall see in Section IV, this is the case for all states obtained by acting with a T -periodic time-dependant scatterer on $|F_{\mu=0}\rangle$.

However, let us recall that this is not true when interactions, for example between the sources and the beam-splitter are present [50]: the depth of the dip is decreased by electronic decoherence. The dip may also not be maximally deep, at zero temperature, when the emission process involves some classical randomness, one example being the randomized train of levitons considered in Section VB 2.

2. Repeated HOM detections

Because electronic atoms of signals are localized in time, they are suitable single-particle states to discuss repeated detection protocols. Let us discuss such a protocol based on two-particle interferometry using an ideal beam splitter with energy-independent transmission probability \mathcal{T} (HOM interferometry).

On one incoming channel, we consider a T -periodic source S whereas on the other incoming channel, we have a specific ideal electronic source S_a which emits a periodic trains of electronic atoms of signals $|\varphi_{a,l}\rangle$, not necessarily related to the ones present emitted by S . Its excess single-electron coherence is thus

$$\Delta\mathcal{G}_{S_a}^{(e)}(t, t') = \sum_{l=0}^N \varphi_{a,l}(t) \varphi_{a,l}^*(t'). \quad (32)$$

The resulting outgoing current noise contains an HOM contribution proportional to the overlap between $\Delta\mathcal{G}_S^{(e)}$ and $\Delta\mathcal{G}_{S_a}^{(e)}$ [45]. Using the T periodicity of $\Delta\mathcal{G}_S^{(e)}$, the experimental signal scales as $N \gg 1$ which quantifies the total acquisition time NT :

$$\int_{[-\frac{NT}{2}, \frac{NT}{2}]^2} \Delta\mathcal{G}_{S_a}^{(e)}(t, t')^* \Delta\mathcal{G}_S^{(e)}(t, t') dt dt' \sim N \bar{p}_a. \quad (33)$$

This overlap counts the number of times an electron in the single-particle state $|\varphi_{a,l}\rangle$ is scattered against an electronic excitation in the same single-particle state for N periods of duration T . Since S_a is an ideal source sending a train of N identical excitations shifted by multiples of T , the quantity \bar{p}_a should be interpreted as the average number of times, the single-particle state φ_a is emitted per period. If the $\varphi_{a,l}$ are among the electronic atoms of signal emitted by S , then when the emission of S_a is synchronized with the emission of these atoms of signal by S , $\bar{p}_a = \bar{g}_a$ is the probability of emission of these electronic atoms of signal by S .

3. Time-frequency filtering

A repeated detection protocol can also be realized by scattering the electron flow through a periodically driven energy-dependent scatterer. Recently, such a time-frequency filtering has been demonstrated and used for single-electron tomography [35]. It relies on a quantum point contact with an energy-dependent transmission probability $T(\omega)$ equipped with a top electrostatic gate driven by a time dependent voltage $V_d(t)$. The signal collected by such a device is the total charge transmitted through the QPC which can be rewritten as a linear filtering of the incident single-electron excess coherence [54]:

$$Q = -e \int_{\mathbb{R}^2} v_F \Delta\mathcal{G}^{(e)}\left(t + \frac{\tau}{2}, t - \frac{\tau}{2}\right) \mathcal{F}_d(t, \tau)^* dt d\tau \quad (34)$$

with the filter's kernel being given by

$$\mathcal{F}_d(t, \tau) = \int_{\mathbb{R}} T(\omega) e^{i\omega\tau + \frac{i\epsilon}{\hbar} \int_{t-\tau/2}^{t+\tau/2} V_d(t') dt'} \frac{d\omega}{2\pi} \quad (35)$$

in which $\mathcal{V}_d(t')$ is proportional to the driving voltage V_d [96].

For a time-periodic driving at frequency $f = 1/T$, the linear filter is also T -periodic. Since $\mathcal{F}_d(t, \tau)^* = \mathcal{F}_d(t, -\tau)$, the Floquet-Bloch analysis can be applied to the filter. Besides the example considered in Ref. [54], the case of a driven quantum dot [55, 56] corresponding to a Lorentzian transmission probability $T(\omega)$ centered at $\omega_0 > 0$ with width $\gamma_0 \ll \omega_0$ is worth considering since it corresponds to a dot filtering mostly electronic excitations around the energy $\hbar\omega_0$. Provided the drive is such that $\omega_0 - eV_d(t)/\hbar \gg \gamma_0$, we expect that only purely electronic excitations are transmitted. We should therefore be able to diagonalize the (dimensionless) filtering operator

$$\mathbf{F}_d = v_F \int_{\mathbb{R}^2} |t_+\rangle \mathcal{F}_d\left(\frac{t_+ + t_-}{2}, t_+ - t_-\right) \langle t_-| dt_+ dt_- \quad (36)$$

within the electronic quadrant, thus leading to:

$$\mathbf{F}_d = \sum_{\alpha} \int_0^{2\pi f} \mathcal{F}_{\alpha}(\nu) |\psi_{\alpha,\nu}^{(d)}\rangle \langle \psi_{\alpha,\nu}^{(d)}| \frac{d\nu}{2\pi} \quad (37)$$

in which the eigenstates $|\psi_{\alpha,\nu}^{(d)}\rangle$ are electronic Floquet-Bloch waves of the filter. The eigenvalues $\mathcal{F}_{\alpha}(\nu)$ are real but (as far as we know) are not restricted. In practice, acquisition of the experimental signal requires a T -periodic single-electron excess coherence $\Delta_0 \mathbf{G}^{(e)}$ and measurement over $N \gg 1$ periods. Then, the total transmitted charge increases linearly with time. The average charge transmitted per period Q_T , and thereby the transmitted dc current $\langle I_{\text{dc}} \rangle = Q_T/T$, can then be expressed in terms of the electronic atoms of signals $|\varphi_{\alpha,l}^{(d)}\rangle$ arising from the Floquet-Bloch waves of the filter. Decomposing

$$\mathbf{F}_d = \sum_{\alpha} \sum_{(l_+, l_-) \in \mathbb{Z}^2} \mathcal{F}_{\alpha}(l - l') |\varphi_{\alpha, l_+}^{(e)}\rangle \langle \varphi_{\alpha, l_-}^{(e)}| \quad (38)$$

in which $\mathcal{F}_\alpha(l_+ - l_-)$ is related to $\mathcal{F}_\alpha(\nu)$ by Eq. (16), leads to the average transmitted dc current:

$$\langle I_{\text{tdc}} \rangle = -ef \sum_\alpha \sum_{l \in \mathbb{Z}} \mathcal{F}_\alpha(l) \langle \varphi_{\alpha,0}^{(d)} | \Delta_0 \mathbf{G}^{(e)} | \varphi_{\alpha,l}^{(d)} \rangle. \quad (39)$$

Therefore, the driven QPC studied in [54] appears as a linear filter acting on linear coherence which generalizes to the time-dependent case, the quantum dot energy filter originally used to study electronic relaxation in quantum Hall edge channels [57]. The average current is then directly proportional to the overlap between $\Delta_0 \mathbf{G}^{(e)}$ and the time-dependent filter's "quantum coherence score" introduced in Section III C. Generically, several bands may be present and therefore several electronic atoms of signal may be needed. However, we can hope that suitable drives may lead to filtering by mostly one band, or equivalently one type of electronic atom of signal thereby enabling us to probe the presence of a specific atom of signal within $\Delta_0 \mathbf{G}^{(e)}$.

IV. MANY-BODY PROPERTIES

Until now, we have focused on the properties of the electronic fluid at the single-particle level, assuming nothing more than T -periodicity. However, when interactions within the electronic fluid can be neglected, the single-particle description actually gives us access to the whole many-body state. This is notably the case when the single-electron source is modelled by single-particle scattering processes.

In this section, we will explain how the Floquet-Bloch analysis allows us to give a simple many-body description and unravel some of the symmetries hidden within the band structure. We will also be able to rederive the single particle scattering operator leading to such a single-electron coherence, thereby exploring the path followed in Ref. [41] the other way around. Furthermore, by giving a direct insight on electron/hole entanglement, the Floquet-Bloch analysis is well suited to quantify the quality of electron sources. We will use it in Section V to identify the best operating experimental parameters for a given source.

A. Many-body state at zero temperature

For the sake of simplicity but without loss of generality, we shall focus on a T -periodic coherence corresponding to a vanishing average dc current so that the chemical potential of the electron fluid is exactly zero, a specific case also considered in [58]. We assume that single electron coherence is the result of T -periodic single-particle scattering $\mu = 0$ Fermi sea ($T_{\text{el}} = 0$ K) $|F\rangle$ which thereby generally describes a T -periodic ac source whenever interactions can be neglected.

In order to derive the many-body state at zero temperature, the method consists into finding an expression

of the many-body Floquet operator from the Floquet-Bloch decomposition (see Appendix E) thereby inverting the procedure described in Refs. [41, 58]. Applying this operator to the Fermi sea leads to the general form of many-body state $|\Psi\rangle$ emitted by the source:

$$\prod_{\substack{\nu \in [0, 2\pi f[\\ a \in \mathbb{N}}} \left(\sqrt{1 - g_a^{(e)}(\nu)} + \sqrt{g_a^{(e)}(\nu)} \psi^\dagger \left[\psi_{a,\nu}^{(e)} \right] \psi \left[\psi_{a,\nu}^{(h)} \right] \right) |F\rangle. \quad (40)$$

From this expression, we notice an important symmetry on the spectrum: because electrons and holes are emitted in pairs, we have $g_a^{(e)}(\nu) = g_a^{(h)}(\nu)$. It is worth noting that this relation is different from electron-hole symmetry, which reverses frequencies and, as such, would be $g_a^{(e)}(\nu) = g_a^{(h)}(2\pi f - \nu)$. Consequently, when electron/hole symmetry is satisfied in state (40), the Floquet-Bloch spectrum exhibits the symmetry: $g_a^{(e)}(\nu) = g_a^{(e)}(2\pi f - \nu)$.

1. The case of flat bands

When the bands are flat, we can go further in the analysis and reexpress the many-body state in terms of Floquet-Wannier wavefunctions. The flat band case ($g_a(\nu) = g_a$) happens for a purely a.c. voltage drive at zero temperature. The case of a.c. voltage drives have been studied previously in [59–61]. In this case, as shown in Appendix E, Eq. (40) can be rewritten as

$$|\Psi\rangle = \prod_{a \in \mathbb{N}} \prod_{l \in \mathbb{Z}} \left(\sqrt{1 - g_a} + \sqrt{g_a} \psi^\dagger \left[\varphi_{a,l}^{(e)} \right] \psi \left[\varphi_{a,l}^{(h)} \right] \right) |F\rangle. \quad (41)$$

This is the formula for a classical voltage drive found in [60]. Since there is no relative phase between $\sqrt{1 - g_g}$ and $\sqrt{g_a} \psi^\dagger [\varphi_{a,l}^{(e)}] \psi [\varphi_{a,l}^{(h)}]$, once a determination for the electronic Floquet-Wannier wavefunctions has been chosen, it determines also the wavefunctions for holes, up to a global phase. As such, we do not expect the Floquet-Wannier wavefunctions to be minimally spread for both electrons and holes. This also allows us to come back to the ansatz guessed in Eq. (8). This ansatz works only in the case of flat bands. While this is the case for a classical drive, we will see that it is usually not the case for the mesoscopic capacitor.

B. Electron/hole entanglement entropy

Accessing the many-body state allows us to quantify the quality of a single-electron (or more generally, a n -electron) source. Such a source would emit electrons and holes independantly, without correlations besides Fermi statistics. Furthermore, because our sources are described as noiseless single-particle scattering from an equilibrium state quantifying outgoing correlations gives

the amount of correlation generated during the scattering process. When the global state is pure ($T_{\text{el}} = 0\text{ K}$), the correlations only come from entanglement.

Although the question of entanglement is a complicated problem in a many-body system [62], the very definition of electron and hole provides us with a natural way to split the many-body Hilbert space in two orthogonal components, thereby enabling us to fall back on a more familiar description. Thanks to the parity super-selection rule for fermions [22–24] and to the absence of superconducting correlations in a metallic conductor, the many-body density operator is block-diagonal, only exhibiting coherences between states having the same number of electron and hole excitations with respect to a reference Fermi sea. Quantifying the electron/hole entanglement could, in principle, be done by looking separately into all these superselection sectors but this would require knowing electronic coherences to all orders.

Fortunately, when Wick's theorem is satisfied, the full many-body state depends only on first-order coherence. This is also true for the partial trace on positive or negative energy states since higher-order correlations functions expressed in frequency basis are just correlation functions of the whole state taken in the simplex of positive frequencies and thereby, they also obey Wick's theorem. From this and the superselection rule follows that the many-body state associated to the electronic quadrant corresponds to filling non-coherently each Floquet-Bloch mode $|\psi_{a,\nu}^{(e)}\rangle$ with its probability $g_a^{(e)}(\nu)$:

$$\hat{\rho}_{++} = \bigotimes_{\substack{\nu \in [0, 2\pi f[\\ a \in \mathbb{N}}} \left((1 - g_a^{(e)}(\nu)) |0\rangle \langle 0| + g_a^{(e)}(\nu) \psi^\dagger[\psi_{a,\nu}^{(e)}] |0\rangle \langle 0| \psi[\psi_{a,\nu}^{(e)}] \right). \quad (42)$$

Its form is reminiscent of a the thermal state with a mode-dependent temperature.

An important property of an ideal n -electron source is that there are no correlations between the electron and hole excitations it emits. Namely, we expect the full many-body state associated to positive and negative frequencies to factorize as $\hat{\rho}_{\text{SES}} = \hat{\rho}_{++} \otimes \hat{\rho}_{--}$. In the present case of a pure many-body state for the whole electronic fluid, the departure from such a factorized form is measured by the von Neumann entanglement entropy of the electrons (or the holes), a quantitative measure of entanglement in this case [63]. Starting from the expression (42) for the many-body state, is it given by

$$S_{\text{vN}} = - \sum_{a \in \mathbb{N}} \int_0^{2\pi f} \left(g_a^{(e)}(\nu) \log_2(g_a^{(e)}(\nu)) + (1 - g_a^{(e)}(\nu)) \log_2(1 - g_a^{(e)}(\nu)) \right) \frac{d\nu}{2\pi f}. \quad (43)$$

Therefore, the entanglement entropy can be inferred from the properties of the Floquet-Bloch spectrum for electrons (or holes) which thereby appears as an entanglement spectrum [64]. This connexion has been exploited

to quantify entanglement between spatially separated regions in many-body fermionic systems or generated by a quantum point contact [65] but can indeed be applied to more general decompositions of the full single-particle state in a sum of two orthogonal components [66].

Finally, at non-zero temperature, the von Neumann entropy is no longer the sole measure of entanglement since the global state is not pure anymore. For practical use in experiments [9], the departure of the full many-body state from a pure state can be quantified using a purity indicator which can also expressed in terms of the Floquet-Bloch electron and hole spectra ($g_a^{(e)}(\nu), g_b^{(h)}(\nu)$) and of electron hole coherences $g_{ab}^{(eh)}(\nu)$ for $0 \leq \nu < 2\pi f$ as detailed in Appendix F.

V. ELECTRON SOURCE ANALYSIS

We now apply our signal-processing technique to numerical data coming from a Floquet modelization of periodic electron sources. Our goal is to use the Floquet-Bloch spectrum to assess the quality of sources as single-electron sources, along the lines discussed in the previous section. Because of their experimental importance, the mesoscopic capacitor [1] and the Leviton source [67] will be discussed. The former offers the possibility to emit single-electron excitations well separated from the Fermi surface. The Leviton source exploits the fact that a suitable rearrangement of an infinite Fermi sea can lead to the generation of purely electronic excitations [68] in a simple way.

A. The mesoscopic capacitor

1. Model

The mesoscopic capacitor depicted on Fig. 2 is modeled using Floquet scattering theory [69], since, in most experimentally relevant regimes, interaction effects within the capacitor itself can be neglected. Within this framework [43, 70], the mesoscopic capacitor is characterized by the level spacing of the dot Δ , the transparency D of the QPC (see Fig. 2) as well as by the voltage drive $V_g(t)$. The Floquet scattering matrix relating the outgoing fermionic field to the incoming one is then expressed as [43, 70]

$$S(t, t') = \exp\left(\frac{ie}{\hbar} \int_{t'}^t V_g(\tau) d\tau\right) \mathcal{S}_0(t - t'), \quad (44)$$

where \mathcal{S}_0 denotes the scattering matrix of the dot which, in the frequency domain, is given by

$$\mathcal{S}_0(\omega) = \frac{\sqrt{1 - D} - e^{2i\pi\hbar(\omega - \omega_0)/\Delta}}{1 - \sqrt{1 - D} e^{2i\pi\hbar(\omega - \omega_0)/\Delta}}, \quad (45)$$

where ω_0 comes from a dc bias applied to the dot. Adjusting it so that $\omega_0 = 0$ ensures that a peak in the density

of states of the dot is located at the Fermi level in the absence of external drive.

We will now discuss the operating regimes of the mesoscopic capacitor operated by a sinusoidal drive $V_g(t) = V \sin(2\pi ft)$ at frequency f by computing the electron/hole entanglement from the Floquet-Bloch spectrum for the electronic excitations at fixed Δ and driving frequency f in terms of the experimentally controlled parameters D and V , the latter being the amplitude of the drive applied to the mesoscopic capacitor. In the present case, we work at fixed drive frequency and dot geometry so that $\Delta/hf \simeq 20$, which corresponds to experimentally realistic conditions. Having in mind the original experiments [1, 71], results for a square drive are given in Appendix G.

2. Electron/hole entanglement entropy

Figure 5 presents a density plot of the entropy defined by Eq. (43) as a function of D and eV/Δ at fixed $\Delta/hf = 20$. There are shallow zones with minima in each square $eV/\Delta \in [n, n+1]$ ($n \in \mathbb{N}$) and $0 < D \leq 1$. A global minimum can be found at eV_{opt}/Δ slightly less than 0.24 and $D_{\text{opt}} \approx 0.38$ and the corresponding entropy is very low: 0.06 bit. As we shall see in Secs. V A 2 and V A 4 this is a regime where the mesoscopic capacitor behaves almost ideally, emitting exactly one electron and one hole excitation per period. Decreasing D from this value leads to a local maximum of the entropy (for $D \simeq 0.11$) before a decrease to zero when $D \rightarrow 0$ corresponding to a regime where the source emits nothing. For each of the three points located at the same value of eV/Δ and corresponding to $D = 0.8$, $D = D_{\text{opt}}$ and $D \simeq 0.11$, the full electronic Wigner distribution function is depicted on Fig. 6. As for the square drive case, interference fringes, characteristic from inter-period electronic coherence as well as for electron/hole coherences, are visible for $D \simeq 0.11$ and to a lesser extent for $D = 0.8$ whereas they are much more discrete for $D = D_{\text{opt}}$.

The local minima on Fig. 5 correspond to quite low values of the electron/hole entanglement entropy. They can also be seen on Fig. 7 presenting cuts for fixed value of D of S_{vN} as functions of eV/Δ . By running a simplex minimization algorithm, we can find position and entropy value at each minimum as summarized on Table I.

There are also local minima in the second square where $1 < eV_D/\Delta \leq 2$ but the corresponding entropy values are higher (above 0.3bit). In this zone we send three electrons and three holes per period. As such, it is not surprising that the purity of the source is lower, since we expect to excite more electron/hole pairs.

3. The Floquet-Bloch spectrum

Let us review the Floquet-Bloch spectra for the three round points marked on Fig. 5. The middle and right

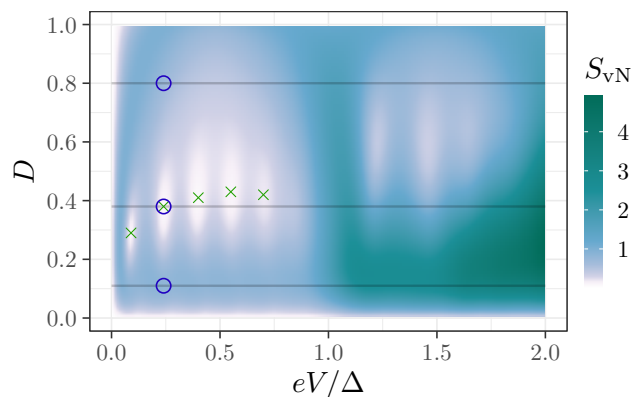


FIG. 5: Density plot of the electron/hole entanglement entropy at zero temperature for the mesoscopic capacitor operated with a sine drive at frequency f such that $\Delta/hf = 20$ as a function of eV/Δ and D . Crosses correspond to the five local minima of the entropy (see Table I) where the source is the closest to an ideal single-electron source. For the second local minimum, we have chosen three values of D : the optimal one, one above and one below (round points) to discuss the effect of varying D for a fixed drive.

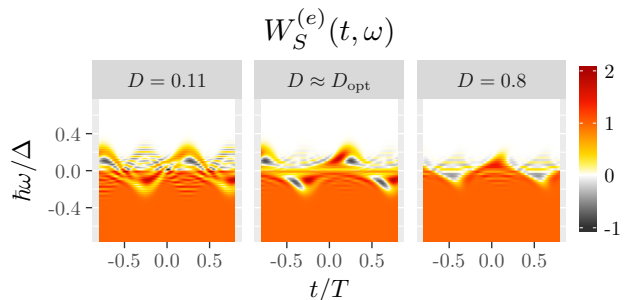


FIG. 6: Density plots of the full Wigner distribution function $W_S^{(e)}(t, \omega)$ for the sine-drive case as a function of t/T and $h\omega/\Delta$ for the three round points appearing on Fig. 5.

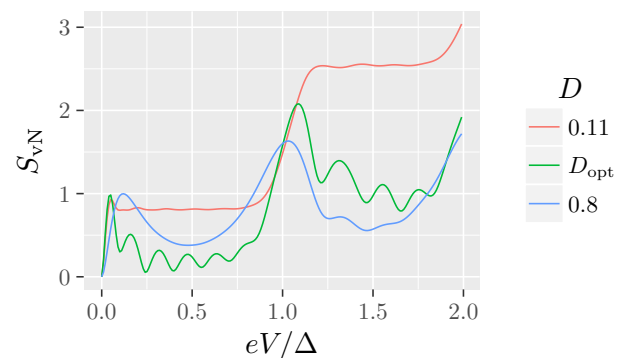


FIG. 7: Cuts of the entropy S_{vN} in the sine-drive case for the three horizontal lines corresponding to $D = 0.11$, $D = D_{\text{opt}}$ and $D = 0.8$ on Fig. 5 as functions of eV/Δ .

TABLE I: Positions in the $(D, eV/\Delta)$ plane and values of S_{vN} (in bits) for the entropy minima – crosses on Fig. 5 – in the sine-drive case for $eV/\Delta \leq 1$ (when about one electron per period is emitted). At each of these operating points, the source emits a single electronic atom of signal per period whose Wigner representation is depicted Fig. 10. The associated hole atom of signal is charge conjugated and shifted by a half-period.

	D	eV/Δ	S_{vN}
1	0.29	0.09	0.10
2	0.38	0.24	0.06
3	0.41	0.40	0.06
4	0.43	0.55	0.10
5	0.42	0.70	0.18

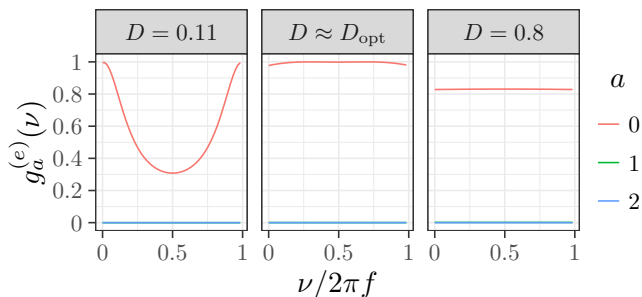


FIG. 8: The Floquet–Bloch spectra for the three selected round points in the sine-drive case appearing on Fig. 5. Only the first three bands are represented, all the other ones being even closer to zero.

panels of Fig. 8 depict flat bands. The middle panel corresponds to the absolute minimum of the entropy, shows one band with average very close to one. This corresponds to the best operating point as a single-electron source. Opening the dot ($D = 0.8$, right panel) also leads to flat bands as expected but we note that the eigenvalues for the first band (which is the only one that is non negligible) is only 0.83.

Going to a closed dot ($D = 0.11$, left panel) leads to a curved first band with average 0.5. This point corresponds to the local maximum of the entropy between $D = 0$ and $D = D_{opt}$ along $eV = eV_{opt}$. At this point, the entropy is equal to 0.85 bit. Starting from the optimal point, decreasing D increases the escape time of the electron and hole excitations. In previous publications [29, 43], we had argued that, in a specific regime, the mesoscopic capacitor emits a quantum superposition of nothing and of an elementary electron/hole pair on top of the Fermi sea. Decreasing D would increase the amplitude of the emission of the electron/hole pair from modulus very close to one to modulus zero and this explains the behavior of the entropy with decreasing D at fixed eV/Δ . However, when D is decreased, inter-period coherences (or equivalently band curvature) appear due electron and hole delocalization over more than one half-

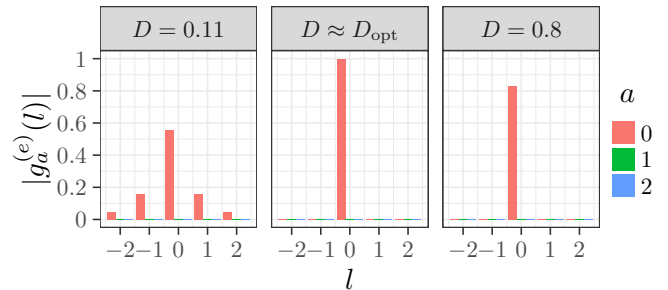


FIG. 9: Modulus of the interperiod coherences $|g_a^{(e)}(l)|$ between the electronic atoms of signal of the $a = 0, 1$ and 2 Floquet–Bloch bands given by Eq. (19) as a function of l for the three round points on Fig. 5 (sine-drive case).

period. This shows how our analysis unravels what happens more precisely than the previously used simple picture.

4. Electronic atoms of signal and coherences

Let us now discuss the electronic atoms of signal as well as their coherence properties at the same three round points. As shown on Fig. 9, for a widely open dot, there is still one type of electronic atom of signal that is emitted per half period, although it is emitted with a probability less than one. When closing the dot, we first encounter an optimal point ($D \sim D_{opt}$) where only one is emitted almost certainly: the mesoscopic capacitor behaves like an almost ideal single-electron source (see Eq. (5)) and there are no inter-period electronic coherences (see Eq. (6)). Finally, when closing the dot, the electronic escape time from the dot increases beyond $T/2$ and, consequently, the elementary electron and hole excitations emitted by the capacitor tend to delocalize over more than one period. Moreover, electron hole coherences are generated and we encounter a point with a local maximum of electron/hole entanglement ($D \simeq 0.11$). Analyzing the shape of the Wannier wavepackets confirms that closing the dot leads to longer wavepackets.

Figure 10 presents the dominant electronic atoms of signal for the local optimal points in the quadrant $0 < D < 1$ and $0 < eV/\Delta < 1$. As we raise the drive amplitude, the Wannier wavefunctions explore higher energies. For each minimum, there is a corresponding number of negative bumps in the Wigner representation. This suggests that these optimal regimes correspond to a resonance between the rising time of the drive voltage, the period and the energy gap of the cavity.

In conclusion, this analysis demonstrates how the Floquet–Bloch analysis can be used to find optimal operating points of single electron sources and, more generally, to characterize what is emitted by the source and to optimize wavepackets shaping strategies [72]. As such,

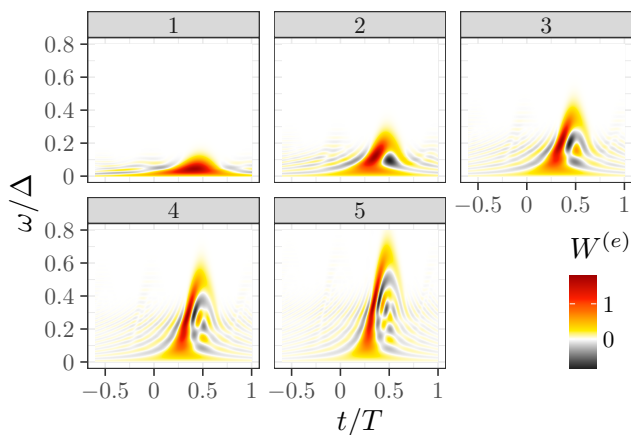


FIG. 10: Dominant electronic atoms of signals emitted by the mesoscopic capacitor for the local minima of S_{v_n} appearing on Fig. 5 (crosses) in the domain $0 < D < 1$ and $0 < eV/\Delta < 1$.

it can help improving the quantitative modeling of many electron quantum optics experiments such as, for example, electronic decoherence experiments [50]. Because the electronic excitations emitted by the mesoscopic capacitor are quite sensitive to this phenomenon, and also for practical reasons, the Leviton sources built from a suitably driven Ohmic contact [67]. We shall now apply our analysis to this very important source.

B. Leviton trains

Let us now consider an Ohmic contact driven by time dependent voltage which is a T -periodic train of Lorentzian pulses of width τ_0 , each of them carrying an electric charge $q = -\alpha e$. The resulting time-dependent voltage

$$V(t) = \frac{\alpha hf}{2e} \frac{\sinh(2\pi f\tau_0)}{\sinh^2(\pi f\tau_0) + \sin^2(\pi ft)} \quad (46)$$

has a d.c. component $V_{dc} = \alpha hf/e$ and an a.c. part $V_{ac}(t) = V(t) - V_{dc}$ [3].

To understand the underlying physics, let us remember what happens in the case of a single Lorentzian pulse of duration τ_0 and integer charge $\alpha = n > 0$ at zero temperature. In this case, the emitted many-body state is a Slater determinant built by adding on the Fermi sea n mutually orthogonal electronic single-electron excitations whose wavefunctions are given in the frequency domain by [73]:

$$\varphi_n(\omega) = \sqrt{4\pi v_F \tau_0} H(\omega) L_{n-1}(2\omega\tau_0) e^{-\omega\tau_0}, \quad (47)$$

where L_n denotes the n th Laguerre polynomial and H is the Heaviside distribution. In the limit where Lorentzian pulses are well separated ($f\tau_0 \ll 1$), we expect the electronic atoms of signal, which we call Levitonoids, to have

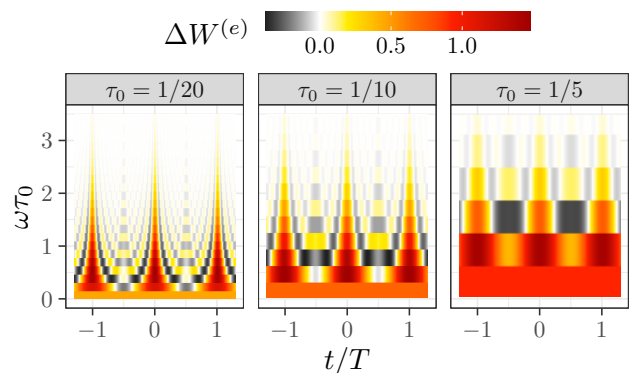


FIG. 11: Wigner distribution function of a Leviton train for different ratio τ_0/T for increasing values of τ_0/T . As we raise τ_0/T , the duration of each Leviton becomes longer and longer and, compared to the energy scale \hbar/τ_0 , hf becomes larger. Once τ_0 is greater than T , the first band of width $2\pi f$, which has no time dependence, is the only one to remain. We are thus left with an almost stationary situation due to the raise of chemical potential by $\delta\mu = hf$.

a strong overlap with these mutually orthogonal wavefunction.

For a Leviton train ($\alpha = 1$), one could naively expect each Lorentzian voltage pulse to carry exactly one Levitonoid excitation. Although, this Levitonoid may tend to the isolated Leviton in the limit $\tau_0 \ll T$, in the case where the Lorentzian pulse start to overlap ($f\tau_0 \gtrsim 1$), the relation between the Levitonoid and the Leviton is non-trivial because of the Pauli principle since single-Leviton wavefunctions of width τ_0 separated by $T \ll \tau_0$ are not orthogonal.

To gain a better understanding of the way information is encoded in such a compact electronic train, besides the periodic train of Levitons, we shall consider in Section VB2 a randomized train of Lorentzian voltage pulses [42], obtained by randomly choosing whether or not each Lorentzian pulse is present in the drive or not. The single-electron coherence associated with this statistical ensemble of voltage drives is still T -periodic and our analysis can be applied.

1. Levitonic atoms of signals

Figure 11 shows the full Wigner distribution function of the T -periodic train of unit charge Lorentzian pulses for different values of $f\tau_0$. Varying this parameter swipes from a dilute train in which each Leviton is well separated from each other, to a compact train in which the pulses are so spread over multiple periods that we only see the variation of the chemical potential due to the d.c. part.

In the $\alpha = 1$ case, Moskalets has obtained explicit expression for electronic atoms of signal associated with such a Leviton train [47]. Each of them leads to a Lorentzian current pulse of width τ_0 . This is manifestly

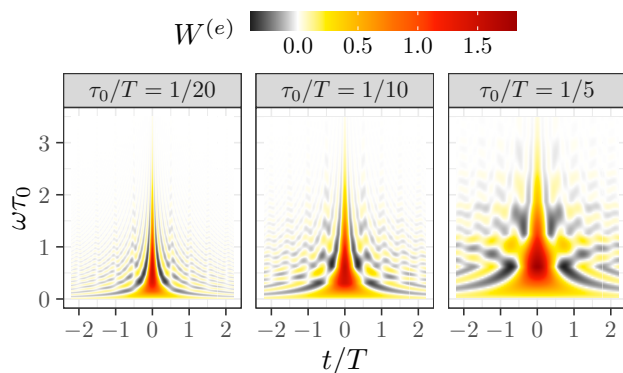


FIG. 12: The electronic atoms of signal of a train of charge α Lorentzian pulses for $\alpha = 1$ and different values of $f\tau_0$. When $f\tau_0 \ll 1$, the wavepacket we obtain is very similar to a Leviton. When $f\tau_0 \simeq 1$, we recover a Martin-Landauer wavepacket. The atoms of signal found by our algorithm (lower panel) fit perfectly the ones predicted analytically (upper panel).

not the case for the electronic atoms of signal obtained numerically whose Wigner representations are depicted on Fig. 12. Our numerical algorithm produces wavepackets having the smallest spreading in time whereas the analytical expressions obtained by Moskalets possess a Lorentzian current pulse of width τ_0 . As shown in Appendix H, an analytical expression for the minimally spread wavepackets can be obtained:

$$\varphi_{\text{Lev}}(\omega) = \frac{1}{\sqrt{\mathcal{N}}} \text{H}(\omega) e^{-\omega_{\text{int}}\tau_0}, \quad (48)$$

where \mathcal{N} is a normalisation factor and $\omega_{\text{int}} = 2\pi f \lfloor \omega/2\pi f \rfloor$ is the frequency counted in multiple of $2\pi f$. This minimally spread Levitonoid is the following linear combination of Martin-Landauer's wavepackets

$$|\text{Lev}\rangle = \sqrt{1 - e^{-4\pi f\tau_0}} \sum_{n=0}^{+\infty} e^{-2\pi n f\tau_0} |\text{ML}_{n,0}\rangle. \quad (49)$$

The details of this derivation can be found in Appendix H. We have checked that this analytical form and the one found by the algorithm match perfectly.

As can be seen from Fig. 12, the minimally-spread Levitonoid tends to the single-Leviton state $|\varphi_1\rangle$ obtained from Eq. (47) in the $f\tau_0 \rightarrow 1$ limit. When we lower $f\tau_0$, the steps of width $2\pi f$ in Eq. (48) become smaller, thereby corresponding to an increasingly closer staircase approximation of the decaying exponential. A measure of the distance between the minimal Levitonoid $|\text{Lev}\rangle$ and the single-Leviton state $|\varphi_1\rangle$ is given by the overlap between these two single-particle states:

$$|\langle \text{Lev} | \varphi_1 \rangle|^2 = \frac{\tanh(\pi f\tau_0)}{\pi f\tau_0} \quad (50)$$

which, for $f\tau_0 \ll 1$, departs quadratically from unity.

In the regime where $f\tau_0 \simeq 1$, the overlap between the minimal Levitonoid and the single Leviton tends to zero as $1/\pi f\tau_0$. In this regime, it seems natural to compare our Levitonoids to the Martin-Landauer wavepacket $|\text{ML}_{1,0}\rangle$ (compare the right panel of Fig. 12 to Fig. 4). This overlap goes exponentially to one as $f\tau_0$ goes to infinity

$$|\langle \text{Lev} | \varphi_{\text{ML}_{0,0}} \rangle|^2 = 1 - e^{-4\pi f\tau_0}. \quad (51)$$

For the examples discussed above, when $f\tau_0 = 1/5$, the overlap is around 92%. At $f\tau_0 = 1$, the overlap is unity up to the sixth significant digit, making the differentiation between a minimally-spread Levitonoid and a Martin-Landauer impossible in practice.

These behaviors shed light on the difference in terms of typical temporal width between the minimally-spread Levitonoids and the wavepackets introduced by Moskalets. For Moskalets' wavepackets, the typical duration is always τ_0 . In our case, the typical duration is τ_0 when $\tau_0 \lesssim T$. However, when $\tau_0 \gtrsim T$, the minimal Levitonoid will have a duration of the order of T and, ultimately, in the $f\tau_0 \rightarrow 0$ limit, tend to a Martin-Landauer wavepacket.

2. The random train

In order to distinguish between the electronic wavepackets used to carry the information and the way they are injected, we elaborate on the recent idea [42] of randomizing the emission process itself. We consider non-periodic trains of electrons associated with infinite random binary chains b_k ($k \in \mathbb{Z}$) which determines whether a Lorentzian pulse centered at $t_k = kT$ is added to the driving voltage ($b_k = 1$ with probability p) or not ($b_k = 0$ with probability $1 - p$):

$$V_d(t) = \sum_{k \in \mathbb{Z}} b_k V_{\text{Lev}}(t - kT) \quad (52)$$

in which $V_{\text{Lev}}(t)$ corresponds to a Lorentzian pulse of width τ_0 carrying a charge $-e$ centered at $t = 0$. Even if pulse emission is randomized, the ensemble average properties of the electron stream are still T -periodic because emission is still centered on times $t_k = kT$ for $k \in \mathbb{Z}$. The average single-electron coherence in the time domain has been evaluated as [42]

$$\mathcal{G}_{R_p}^{(e)}\left(t + \frac{\tau}{2} \middle| t - \frac{\tau}{2}\right) = \frac{\sin[\pi(ft - \theta_p(f\tau))] \sin[\pi(ft + \theta_p(f\tau))]}{\sin[\pi f(t - i\tau_0 + \frac{\tau}{2})] \sin[\pi f(t + i\tau_0 - \frac{\tau}{2})]} \mathcal{G}_F^{(e)}(\tau) \quad (53)$$

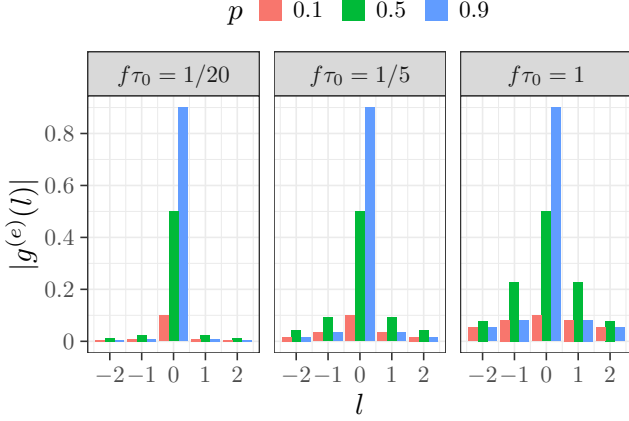


FIG. 13: Coherence between time-shifted Levitonoids for the random train with emission probabilities $p = 0.1, 0.5, 0.9$ and a width $f\tau_0 = 1/20, 1/5, 1$. The central peak has value p and we clearly see the increase of inter-period coherences when increasing $f\tau_0$ at fixed p and their spreading when decreasing p at fixed $f\tau_0$.

in which the index R_p stands for “randomly emitted with probability p ”, $\mathcal{G}_F^{(e)}$ denotes the Fermi sea’s single-electron coherence and

$$\theta_p(x) = \sqrt{\frac{x^2}{4} - (f\tau_0)^2 - i(1-2p)f\tau_0 x}. \quad (54)$$

Eqs. (53) and (54) are the starting point for applying our Floquet–Bloch analysis for finding the electronic atoms of signals underlying the randomized train of Lorentzian pulses. Remarkably, the analysis can be performed numerically but also analytically, as explained in Appendix I.

The first important result is that the excess single-electron coherence can be described in terms of minimal Levitonoids which are the appropriate electronic atoms of signal for the non-random T -periodic train. This illustrates quantitatively the motivation put forward in [42]: randomization enables us to separate what is emitted from the way it is emitted. Single electron coherence is thus described in terms of the same electronic atoms of signals but with a different “quantum coherence score”.

More precisely, when the pulses are widely spaced ($f\tau_0 \ll 1$), we can associate a single-electron excitation (the minimal Levitonoid) which is very close to the Leviton wavepacket (see Eq. (50)) with each Lorentzian pulse. Lowering p then just lowers the emission probability of the corresponding single-electron excitation (see the left panel of Fig. 13). In this regime, randomization just low-

ers the intensity of the emission, as would be expected with a classical ensemble of musicians choosing to play, or not to play, one of the periodically repeated note from the “I Gotta Feeling” music score.

However, for the random Leviton train, lowering the emission probability of each Lorentzian pulses can lead to subtle effects when the Pauli principle starts to enter the game, in the $f\tau_0 \sim 1$ regime or above. This is the second important result from our detailed analysis: although, the excess single-electron coherence is still described in terms of minimal Levitonoids, lowering p also introduces inter-period coherences depicted on Fig. 13. At fixed p , they increase with $f\tau_0$ as seen by comparing the three panels of Fig. 13. In this regime, the modification of the “quantum coherence score” induced by lowering p is not naively classical as in the $f\tau_0 \ll 1$ regime: interperiod coherences are revealed. This can be understood as follows: the limit of a dense T -periodic train is recovered for $p \rightarrow 1$: one Levitonoid is then emitted per period without any inter-period coherences. But then, decreasing p opens some space on the adjacent periods: among all the classical drives building the statistical ensemble underlying R_p , the weight of those containing pulses separated by more than T increases and this contributes to the increasing weight of inter-period coherences. In the limit $p \rightarrow 0$, we thus expect to recover an excess electronic coherence spreading over $|\tau| \lesssim \tau_0$, very similar to the one of an isolated Leviton because, in this limit, the weight of trajectories for which an emitted Lorentzian pulse is separated from the nearest other emitted pulses by more than τ_0 goes to unity. This explains the increasing inter-period coherences in the low p , high $f\tau_0$ regime.

Remarkably, and this is the third result from our in-depth analysis, these interperiod coherences can be recasted in terms of normalized single-electron states, which we call the p -Glattlion and which are

$$|\text{Gla}_p\rangle = \int_0^{+\infty} \sqrt{\frac{1 - e^{-4\pi f\tau_0}}{pf}} e^{-\omega_{\text{int}}\tau_0} \sqrt{g^{(e)}(\omega)} |\omega\rangle d\omega. \quad (55)$$

Using these single-particle states, the excess single-electron coherence can be written as

$$\Delta_0 \mathbf{G}_{R_p}^{(e)} = p \sum_{l \in \mathbb{Z}} |\text{Gla}_{p,l}\rangle \langle \text{Gla}_{p,l}| \quad (56)$$

in which $|\text{Gla}_{p,l}\rangle = \mathbf{T}_T^l |\text{Gla}_p\rangle$ is the p -Glattlion translated by lT . This rewriting resums the interperiod coherences in the minimal Levitonoid basis into pure single-electron states. Ultimately, such a rewriting reflects the coherence of the voltage pulses trains used to build the random ensemble R_p . The price to pay is that these

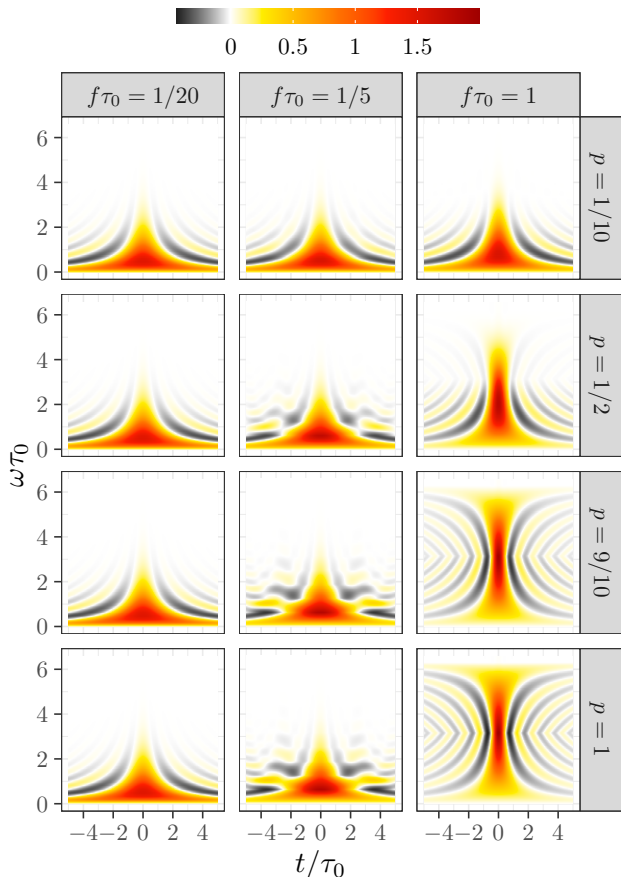


FIG. 14: Wigner representations of p -Glattlions for $p = 0.1, 0.5, 0.9, 1$ and a width $f\tau_0 = 1/20, 1/5$ and 1 . The case $p = 1$ corresponds to the minimal Levitonoids introduced in Section VB 1. Note that, on this figure, time is counted in units of τ_0 so that we clearly see how the p -Glattlion interpolates between a Leviton-like Wigner representation of width τ_0 for $p = 1/10$ to a minimal Levitonoid one for $p = 9/10$.

states cannot be viewed as electronic atoms of signals since they are not mutually orthogonal between different periods (see Eq. (I18)). The Wigner representations of Gla_p for various $(p, f\tau_0)$ are plotted on Fig. 14. These single-particle states interpolate between Leviton wavefunctions of width τ_0 in the limit $f\tau_0 \ll 1$ or $p \ll 1$ and the minimal Levitonoid obtained for $p = 1$.

VI. CONCLUSION AND PERSPECTIVES

In this work, we have introduced a representation of the single-electron coherence of a periodic electron source in terms of perfectly distinguishable normalized single-particle wavefunctions associated with each period which we call “electronic atoms of signals” [29]. This description, which is the counterpart of the Karhunen-Loève decomposition for classical signals [74], enables us to obtain a simple description of the single-particle content emitted

by the source in discrete terms. The electronic atoms of signal are the building blocks of the single-electron coherence which are emitted according to their emission probabilities and quantum coherences. Such a decomposition is very reminiscent of the way music can be described in terms of notes arranged along a specific score: the emission probability being the analogous of the strength at which the note is played whereas the coherences are specifically quantum. This type of decomposition, generalized to non-periodic quantum electrical currents is a convenient way to represent general single-electron quantum signals exactly as a music score represents a generically non-periodic piece of music. This is the appropriate framework to discuss the encoding and decoding of the quantum information embedded within a quantum electrical current.

Being able to access the single-particle content of a quantum electric current suggests that a very high degree of control may be envisioned in the near future. This is particularly important for the potential applications of electron quantum optics to quantum sensing of electromagnetic fields on a sub-micrometric space and sub-nanosecond time scale.

In particular, our study of electron sources also shows that, generically, an electron source emits several electron or hole wavefunctions. The multiplicity of emitted excitations is enhanced by non-zero temperature as shown in the recent experimental study [9]. From a signal processing point of view, this means that in general, electron quantum optics sources and detectors respectively emit and detect many different electron and hole excitations. In this sense, they are quantum counterparts to MIMO (Multiple-Input Multiple-Output) classical microwave devices such as advanced radars and Wi-Fi routers, which make use of many (spatial) modes to improve transmission or detection performances. In the long run, the representation of electronic coherence in terms of electronic atoms of signal will be instrumental for characterizing and improving the performances of quantum sensing devices based on quantum electric currents, exactly as MIMO is now used in radar technology [75]. It may as well help quantifying and maybe improving quantum information flow within these devices, as was done in classical signal processing [76].

This decomposition may also bring new insights on physical phenomena such as electron fractionalization [73, 77], the effect of temperature on trains of multiparticle states [78] and interaction-induced electronic decoherence [50, 79]. Since the Floquet-Bloch decomposition provides a zero-order guess for the many-body state from single-particle coherence in the absence of interactions, it is the perfect starting point for a more refined description of the many-body states based, for example, on the adaptation to electron quantum optics of the unitary coupled cluster method now used in variational quantum eigensolvers [80]. Such an ansatz would reproduce deviations from Wick’s theorem at higher and higher order coherences, thereby providing a clear insight

of the electronic coherences in terms of the many-body state.

Finally, our quantum analyzer may also offer a way to access to the recently studied electron/hole entanglement [81–83] and, supplemented by other measurements [28], to quantify more precisely the importance of interaction-induced higher order quantum correlations as well as of thermal fluctuations [84, 85].

The general quantum signal processing method presented here is also directly relevant for electron quantum optics in other systems such as topological insulators [86] and, with some adaptation, in strongly correlated 1D quantum edge channels such as fractional quantum Hall edges [87] where it might shed some light on recently predicted correlation effects within trains of Lorentzian pulses [88]. Finally, it can establish a bridge between electron and microwave quantum optics [89–92], by probing the electronic content of microwave photons injected from a transmission line into a quantum conductor. However, this requires establishing a bridge between the coherence properties of electrons and the quantum optical coherence of the emitted radiation extending the work of Ref. [93].

Acknowledgments

We thank E. Bocquillon, P. Borgnat and P. Flandrin for useful discussions. This work is supported in part by the ANR grant “1shot reloaded” (ANR-14-CE32-0017), the ERC Consolidator grant “EQUO” and by the Joint Research Project “SEQUOIA” (17FUN04) within the European Metrology Programme for Innovation and Research (EMPIR) co-financed by the Participating States and from the European Union’s Horizon 2020 research and innovation programme.

Appendix A: Normalizations

The single-particle states $|t\rangle$ and $|\omega\rangle$, normalized as

$$\langle t|t'\rangle = v_F^{-1} \delta(t-t') \quad (\text{A1a})$$

$$\langle \omega|\omega'\rangle = \delta(\omega-\omega') \quad (\text{A1b})$$

are related by

$$|t\rangle = \frac{1}{\sqrt{2\pi v_F}} \int d\omega e^{i\omega t} |\omega\rangle \quad (\text{A2a})$$

$$|\omega\rangle = \sqrt{\frac{v_F}{2\pi}} \int dt e^{-i\omega t} |t\rangle \quad (\text{A2b})$$

Using the expression of the fermion field operator

$$\psi(t) = \int_{\mathbb{R}} c(\omega) e^{-i\omega t} \frac{d\omega}{\sqrt{2\pi v_F}} \quad (\text{A3})$$

in terms of fermionic annihilation and creation operators $c(\omega)$ $c^\dagger(\omega)$ obeying the canonical anticommutation relations $\{c(\omega), c^\dagger(\omega')\} = \delta(\omega-\omega')$, the $\mathbf{G}^{(e)}$ operator is

expressed in the $|\omega\rangle$ base as

$$\mathbf{G}^{(e)} = \int_{\mathbb{R}^2} |\omega_+\rangle \langle c^\dagger(\omega_-) c(\omega_+) \rangle_\rho \langle \omega_-| d\omega_+ d\omega_- . \quad (\text{A4})$$

Appendix B: Floquet-Bloch theory

1. Diagonalizing the electron part

Let us introduce the projectors $\mathbf{\Pi}_\pm$ on the space of positive (resp. negative) energy single-particle states. The projections $\mathbf{G}_{\varepsilon,\varepsilon}^{(e)} = \mathbf{\Pi}_\varepsilon \mathbf{G}^{(e)} \mathbf{\Pi}_\varepsilon$ ($\varepsilon = \pm 1$) of the single-electron coherence operator contain information on electronic excitations for $\varepsilon = +$ and on hole excitations for $\varepsilon = -$. These correspond to the electron and hole quadrants of Fig. 3. In the same way, the off-diagonal parts $\mathbf{G}_{\varepsilon,-\varepsilon}^{(e)} = \mathbf{\Pi}_\varepsilon \mathbf{G}^{(e)} \mathbf{\Pi}_{-\varepsilon}$ couple the electron and hole parts of the single-particle state and encode electron/hole coherences.

Note that $\mathbf{G}_{++}^{(e)}$ contains all the electronic excitations, even the thermal ones that are present at non-zero temperature when the source is switched off. Keeping these is essential for having positive operators to diagonalize. Denoting by $\Delta_0 \mathbf{G}_{(e)} = \mathbf{G}^{(e)} - \mathbf{G}_F^{(e)} = \mathbf{G}^{(e)} - \mathbf{\Pi}_-$, we have

$$\mathbf{G}^{(e)} = \mathbf{\Pi}_- + \mathbf{G}_{++}^{(e)} + \Delta_0 \mathbf{G}_{--}^{(e)} + \mathbf{G}_{+-}^{(e)} + \mathbf{G}_{-+}^{(e)} \quad (\text{B1})$$

where $\mathbf{G}_{--}^{(e)} = \mathbf{\Pi}_- + \Delta_0 \mathbf{G}_{--}^{(e)}$ and $\mathbf{G}_{++}^{(e)} = \Delta_0 \mathbf{G}_{++}^{(e)}$ (same for $+-$ and $-+$).

The first step consists in diagonalizing the electron part of the excess single-electron coherence $\mathbf{G}_{++}^{(e)}$. Since $\mathbf{G}^{(e)}$ is hermitian as well as $\mathbf{\Pi}_+$, $\mathbf{G}_{++}^{(e)}$ is also hermitian. Since $[\mathbf{\Pi}_+, \mathbf{T}_T] = 0$, $\mathbf{G}_{++}^{(e)}$ commutes with \mathbf{T}_T and we also know that it is a positive operator bounded by 1. Therefore, $\mathbf{G}_{++}^{(e)}$ and \mathbf{T}_T can be diagonalized simultaneously. Exactly as in solid state theory, the diagonalization is performed on each of the eigenspaces of \mathbf{T}_T which consist in quasi-periodic single-particle states associated with a quasi-energy $0 \leq \nu < 2\pi f\mathbb{Z}$ ($f = 1/T$) and corresponding to the eigenvalue $e^{-i\nu T}$ of \mathbf{T}_T . The spectrum for $\mathbf{G}_{++}^{(e)}$ has a band structure with eigenvalues $g^{(e)}(\nu) \in [0, 1]$ for $0 \leq \nu < 2\pi f$. We can therefore find an orthogonal basis of eigenvectors $|\psi_{a,\nu}^{(e)}\rangle \in \mathcal{H}_+$ such that

$$\mathbf{T}_T |\psi_{a,\nu}^{(e)}\rangle = e^{-i\nu T} |\psi_{a,\nu}^{(e)}\rangle \quad (\text{B2a})$$

$$\mathbf{G}_{++}^{(e)} |\psi_{a,\nu}^{(e)}\rangle = g_a^{(e)}(\nu) |\psi_{a,\nu}^{(e)}\rangle \quad (\text{B2b})$$

These eigenvectors are called the electronic Floquet-Bloch vectors and we can choose them to satisfy the normalization conditions

$$\langle \psi_{a,\nu}^{(e)} | \psi_{a',\nu'}^{(e)} \rangle = 2\pi \delta_{a,a'} \delta(\nu - \nu') \quad (\text{B3})$$

which is the same as the $\sqrt{2\pi} |\omega\rangle$ states. The explicit form of the eigenvalue equations used in the numerical

computation is discussed in Appendix B4. It relies on the decomposition of each Floquet-Bloch state as a sum of plane waves whose energies differ by a multiple of hf :

$$|\psi_{a,\nu}^{(e)}\rangle = \sum_{n=0}^{+\infty} u_{a,\nu}^{(n)} |\nu + 2\pi n f\rangle. \quad (\text{B4})$$

The main difference with the usual Bloch theory in solid state physics comes from the fact that, here, the sum is restricted to $n \in \mathbb{N}$ because we are considering electronic excitations.

2. Hole excitations and electron/hole coherences

Having discussed the electronic part of the single-electron coherence, let us discuss the hole part as well as the electron/hole part. We can introduce a hole operator $\mathbf{G}^{(h)}$ defined by replacing $\mathcal{G}_{\rho,x}^{(e)}(t,t')$ in Eq. (11) by

$$\mathcal{G}_{\rho,x}^{(h)}(t,t') = \text{tr}(\psi^\dagger(x,t) \rho \psi(x,t')). \quad (\text{B5})$$

This operator satisfies the same mathematical properties as $\mathbf{G}^{(e)}$. This can be easily shown by using the anti-commutation relations of fermionic operators to relate electron and hole coherence operators:

$$\mathbf{G}^{(h)} = \mathbf{1} - \mathbf{C}\mathbf{G}^{(e)}\mathbf{C}^\dagger, \quad (\text{B6})$$

where \mathbf{C} is the anti-unitary involution that transforms electrons in holes and vice-versa, defined in the time basis by complex conjugation: $\langle t|\mathbf{C}\psi\rangle = \langle t|\psi\rangle^*$. We then have $\mathbf{G}^{(h)} = \mathbf{\Pi}_- - \mathbf{C}\Delta_0\mathbf{G}^{(e)}\mathbf{C}^\dagger$ and therefore, holes can be dealt with along the same lines as electronic excitations.

However, rather than focusing on the restriction of $\mathbf{G}^{(h)}$ to the positive frequencies quadrant, it turns out to be more convenient to focus on $\Delta_0\mathbf{G}^{(e)}$ defined as the restriction to the negative frequencies quadrant of $\Delta_0\mathbf{G}^{(e)} = \mathbf{G}^{(e)} - \mathbf{\Pi}_-$. Taking differences with respect to the $\mu = 0$ Fermi sea ensures that all excitations, including thermal ones, are taken into account. Then $\Delta_0\mathbf{G}^{(e)}$ contains eigenfunctions of holes at negative frequencies, with eigenvalues that are the opposite of hole occupation numbers.

Exactly as $\mathbf{G}_{++}^{(e)}$, $\mathbf{G}_{--}^{(e)}$ can be diagonalized simultaneously with \mathbf{T}_T . We thus introduce an eigenbasis of hole single-particle states $|\psi_{b,\nu}^{(h)}\rangle \in \mathcal{H}_-$ such that

$$\Delta_0\mathbf{G}_{--}^{(e)} = - \sum_b \int_0^{2\pi f} g_b^{(h)}(\nu) |\psi_{b,\nu}^{(h)}\rangle \langle \psi_{b,\nu}^{(h)}| \frac{d\nu}{2\pi}. \quad (\text{B7})$$

Using the completion relation

$$\mathbf{\Pi}_- = \sum_b \int_0^{2\pi f} |\psi_{b,\nu}^{(h)}\rangle \langle \psi_{b,\nu}^{(h)}| \frac{d\nu}{2\pi}, \quad (\text{B8})$$

the hole part $\mathbf{G}_{--}^{(e)}$ is then diagonal in the $|\psi_{b,\nu}^{(h)}\rangle$ basis with respective eigenvalues $1 - g_b^{(h)}(\nu)$:

$$\mathbf{G}_{--}^{(e)} = \sum_b \int_0^{2\pi f} (1 - g_b^{(h)}(\nu)) |\psi_{b,\nu}^{(h)}\rangle \langle \psi_{b,\nu}^{(h)}| \frac{d\nu}{2\pi}. \quad (\text{B9})$$

This convention for the hole Floquet-Bloch spectrum ensures that $\mathbf{G}_{++}^{(h)}$ is diagonalized by the eigenvectors $\mathbf{C}|\psi_{b,\nu}^{(h)}\rangle$ with respective eigenvalue $g_b^{(h)}(\nu)$. Let us notice that, for $0 \leq \nu < 2\pi f$, the hole eigenstate decomposition into plane wave takes the form

$$|\psi_{b,\nu}^{(h)}\rangle = \sum_{n=1}^{+\infty} v_{b,\nu}^{(n)} |\nu - 2\pi f n\rangle \quad (\text{B10})$$

in order to include only negative energy plane waves. The final step for deriving Eq. (15) is to introduce the electron/hole coherences in the basis of electronic and hole Floquet-Bloch eigenstates:

$$\langle \psi_{a,\nu}^{(e)} | \mathbf{G}^{(e)} | \psi_{b,\nu'}^{(h)} \rangle = 2\pi \delta(\nu - \nu') g_{ab}^{(eh)}(\nu) \quad (\text{B11a})$$

$$\langle \psi_{b,\nu}^{(h)} | \mathbf{G}^{(e)} | \psi_{a,\nu'}^{(e)} \rangle = 2\pi \delta(\nu - \nu') g_{ba}^{(he)}(\nu) \quad (\text{B11b})$$

3. Floquet-Bloch eigenvalues as occupation numbers

The normalization condition (14) for the eigenstates $|\psi_{a,\nu}^{(e)}\rangle$ is the same as the one of plane waves except for the fact that, in the present case, ν is a quasi-momentum living in $\mathbb{R}/2\pi f\mathbb{Z}$. The destruction operator associated with such an excitation is thus defined by direct analogy with the operator $c(\omega)$:

$$\psi[\psi_{a,\nu}^{(e)}] = \frac{v_F}{\sqrt{2\pi}} \int_{-\infty}^{+\infty} \psi_{a,\nu}^{(e)}(t)^* \psi(t) dt, \quad (\text{B12})$$

where the normalization factor ensures the canonical anti-commutation relation

$$\{\psi[\psi_{a,\nu}], \psi^\dagger[\psi_{a',\nu'}]\} = \delta_{a,a'} \delta(\nu - \nu'). \quad (\text{B13})$$

It then follows that

$$\langle \psi^\dagger[\psi_{a',\nu'}] \psi[\psi_{a,\nu}] \rangle = \delta_{a,a'} \delta(\nu - \nu') g_a^{(e)}(\nu). \quad (\text{B14})$$

This equation is analogous to the expression of the single-electron coherence of a stationary state in the basis of fixed energy single particle states $|\omega\rangle$ in terms of the electron distribution function $f_e(\omega)$:

$$\langle c^\dagger(\omega') c(\omega) \rangle = \delta(\omega - \omega') f_e(\omega). \quad (\text{B15})$$

The eigenvalues $g_a^{(e)}(\nu)$ can thus be interpreted as the occupation numbers of the single-particle states $|\psi_{a,\nu}^{(e)}\rangle$. We can therefore interpret the spectrum of $\mathbf{G}_{++}^{(e)}$ as bands of

occupation numbers for the Floquet-Bloch states $|\psi_{a,\nu}^{(e)}\rangle$ as a function of their quasi-energy $\nu \in \mathbb{R}/2\pi f\mathbb{Z}$. In the same way, the bands $\nu \mapsto g^{(h)}(\nu)$ can be interpreted as giving the occupation numbers for the hole excitations $\mathbf{C}|\psi_{b,\nu}^{(h)}\rangle$ which are quantum superpositions of single particle states with energies $hf - \hbar\nu$ shifted by positive multiples of hf .

Of course, this raises the question of the band structure that can occur in this type of problem. In order to get a hint on this question, we must have a closer look at the underlying eigenvalue problems.

4. Eigenvalue equations

The diagonalization problem that leads to the spectrum $(g_a(\nu))_{a,\nu}$ and to the Floquet-Bloch eigenfunctions is best expressed in the frequency domain [43, 45]. Exactly as in Bloch's theory, we introduce T -periodic dimensionless functions $u_{a,\nu}$ such that $\psi_{a,\nu}(t) = e^{-i\nu t} u_{a,\nu}^{-1/2}(t)$. Choosing a representative of the quasi-energy $\nu \in [0, 2\pi f[$, we decompose $u_{a,\nu}(t)$ in Fourier series

$$u_{a,\nu}(t) = \sum_{n=0}^{+\infty} u_{a,\nu}^{(n)} e^{-2i\pi nft}. \quad (\text{B16})$$

where the sum goes from $n = 0$ to $n = +\infty$ since we are looking for purely electronic wavefunctions so each $\nu + 2\pi nf$ is positive. The eigenvalue equation $\mathbf{G}_{++}^{(e)}|\psi_{a,\nu}\rangle = g_a^{(e)}(\nu)|\psi_{a,\nu}\rangle$ can then be rewritten in terms of the single-electron coherence projected onto the electron quadrant. With our choice of a representative $\nu \in [0, 2\pi f[$ for the quasi-energy, the eigenvector equation for $g_a^{(e)}(\nu)$ is

$$\sum_{p \in \mathbb{N}} W_{++}^{(e)}(\nu + \pi f(n+p)) u_{a,\nu}^{(p)} = g_a^{(e)}(\nu) u_{a,\nu}^{(n)}. \quad (\text{B17})$$

where, because of T -periodicity, we have decomposed the Wigner distribution function $W_{++}^{(e)}(t, \omega)$ associated with $\mathbf{G}_{++}^{(e)}$ as a Fourier series:

$$W_{++}^{(e)}(t, \omega) = \sum_{n \in \mathbb{Z}} e^{-2\pi inft} W_{++}^{(e)}(\omega) \quad (\text{B18})$$

Note that, because we are considering the projection onto the electronic quadrant, $W_{++}^{(e)}(\omega) = 0$ for $\omega - \pi|n|f < 0$ and equal to $W_n^{(e)}(\omega)$ the n -th harmonic of the full Wigner function, for $\omega - \pi|n|f \geq 0$. Eq. (B17) is solved numerically to determine the spectrum of the single-electron coherence restricted to the electronic quadrant. We can also see it as the diagonalization of the matrix $M(\nu)$, defined for each $\nu \in [0, 2\pi f[$ as

$$M_{np}(\nu) = W_{++}^{(e)}(\nu + \pi f(n+p)) \quad (\text{B19})$$

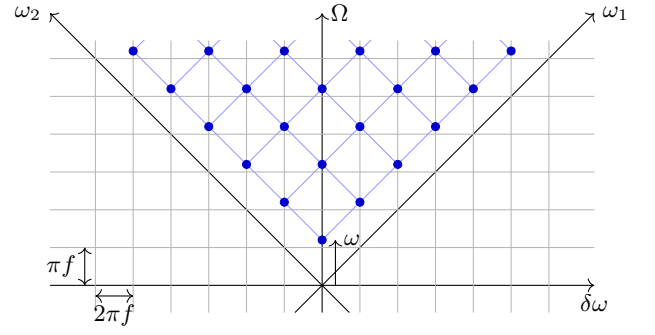


FIG. 15: Graphical representation of the matrix $M(\nu)$. The first-order coherence in energy representation takes values for $\delta\nu$ being an integer multiple of $2\pi f$. The matrix we extract at a given frequency ν is the one given by the value of the blue dots, that are spaced by $2\pi f$ in both vertical and horizontal direction. Shifting the frequency ν by $\delta\nu$ corresponds to vertically translating all blue dots by $\delta\nu$.

for $(n, p) \in \mathbb{N}^2$. This matrix is thus derived from the energy representation of the first-order coherence as graphically pictured on Fig. 15.

The eigenvalues for the hole Floquet-Bloch matrix are obtained in the same way starting from (B10) and following the same step very precisely. This leads to the eigenvalue equation ($0 \leq \nu < 2\pi f$ and $n \in \mathbb{N}^*$):

$$\sum_{p=1}^{+\infty} W_{--}^{(e)}(\nu - \pi f(n+p)) v_{b,\nu}^{(p)} = (1 - g_b^{(h)}(\nu)) v_{b,\nu}^{(n)} \quad (\text{B20})$$

in which

$$W_{--}^{(e)}(t, \omega) = \sum_{n \in \mathbb{Z}} e^{-2\pi inft} W_{--}^{(e)}(\omega) \quad (\text{B21})$$

is the Wigner distribution function associated with $\mathbf{G}_{--}^{(e)}$ and therefore $W_{--}^{(e)}(\omega) = 0$ for $\omega + \pi|n|f > 0$ and is equal to $W_n^{(e)}(\omega)$ as soon as $\omega + \pi|n|f \leq 0$.

5. Case of a voltage drive at zero temperature

A specific feature of the case of a time-dependent classical drive is that, at zero temperature, the energy coherence is piecewise constant, the width of each step being $2\pi f$. If we consider a purely a.c. drive, the discontinuities does not appear when we extract the matrix $M(\nu)$ for $\nu \in [0, 2\pi f[$ (see Fig. 16, left). As such, the eigenvalues will be independent on the quasi-energy, and the eigenvectors of different quasi-energy can be deduced by a frequency translation. It implies notably that it is possible to find a set of Floquet-Wannier functions that are piecewise constant in energy, with discontinuities happening every $2\pi f$. Consequently, the electronic atoms of signal are linear combinations of Martin-Landauer wavepackets, a point already noticed in Ref. [3], and there are no inter-period coherences due to band flatness.

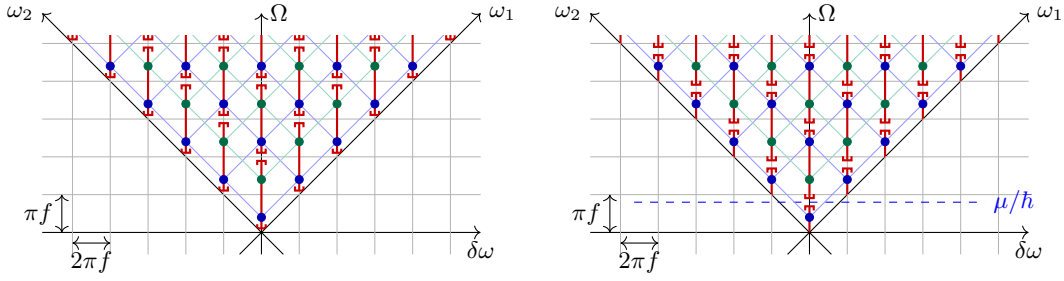


FIG. 16: Matrices for a voltage drive at zero temperature. On the left, the case of an a.c. voltage drive. In this case, the coherence is constant for all $\nu \in [0, 2\pi f[$. The eigenvalue problem does not depend anymore on the quasi-energy. On the right, we consider that there is a d.c. part on top of the a.c. voltage. In this case, the matrix $M(\nu)$ will be piecewise constant, with a step at $\nu = \mu/\hbar \pmod{2\pi f}$.

If we add a d.c. part to the voltage, then it will shift the whole energy coherence by μ/\hbar (see Fig. 16, right). In this case, there are two possibilities:

- If μ/hf is an integer, we are back to the a.c. case, since the discontinuity will not happen for $\nu \in [0, 2\pi f[$.
- If μ/hf is not an integer, then the matrix $M(\nu)$ will be piecewise constant, with a step at $\nu = \mu/\hbar [2\pi f]$. Similarly, the eigenvectors for $\nu \in [0, \omega_s[$ can be deduced by translating the eigenvectors at $\nu = 0$ in energy. The eigenvectors for $\nu \in [\omega_s, 2\pi f[$ can be deduced by translating the eigenvectors at ω_s . In this case, we can find a set of Floquet-Wannier functions that are piecewise constant in energy, with steps happening at $2\pi n f$ and $2\pi n f + \omega_s$.

If we consider a small, non-zero temperature, such that $k_B T_{el} \ll hf$, the steps will be smoothed out over a scale $k_B T_{el}/\hbar$. We can thus expect that the property mentioned above remains true, except at the neighborhood of discontinuities.

This example demonstrates that, contrary to the case of bands in solid state physics, the Floquet-Bloch bands we are considering here may exhibit discontinuities that, indeed, may play a crucial role. For example, this is the case when applying a dc-voltage bias corresponding to a non-integer multiple of $-ef$ dc current to an ac voltage drive or, more generally, to a purely ac-source. An example is a periodic train of Lorentzian voltage pulses carrying a non integer charge in units of $-e$.

Appendix C: Floquet-Wannier function ambiguities

In this Appendix, we discuss the ambiguities in the determination of electronic atoms of signals and propose a minimal-spreading principle for selecting a specific choice of electronic atoms of signals.

1. Origin of the ambiguities

Ambiguities in the choice of Floquet-Wannier wavefunctions can always be traced back to degenerate common eigenspaces for $\mathbf{G}_{++}^{(e)}$ and \mathbf{T}_T . Let us introduce a unitary transformation \mathbf{U} that keeps $\mathbf{G}_{++}^{(e)}$ eigenspaces stable: $[\mathbf{U}, \mathbf{G}_{++}^{(e)}] = 0$, then using the $\mathbf{U}|\psi_{a,\nu}\rangle$ states in (16), we obtain a new orthonormal family of Wannier functions which we denote by $|\varphi_{a,l}^{[U]}\rangle$. Equation (17) becomes

$$\mathbf{T}_T |\varphi_{a,l}^{[U]}\rangle = |\varphi_{a,l+1}^{[\mathbf{T}_T \mathbf{U} \mathbf{T}_T^\dagger]}\rangle. \quad (\text{C1})$$

In order to satisfy the time-translation property of Wannier wavefunctions (17), we require that \mathbf{U} preserves each eigenspace of \mathbf{T}_T and we will then discuss what happens depending on the structure of the common eigenspaces of \mathbf{T}_T and $\mathbf{G}_{++}^{(e)}$.

Preserving the eigenspaces of \mathbf{T}_T immediately implies that \mathbf{U} preserves quasi-energy eigenspaces. Assuming that it leaves each of them invariant, this means that it reduces to a unitary transformation operating on the space generated by all the Floquet-Bloch states at a given quasi-energy. Let us now analyze what happens depending on the eigenspaces of $\mathbf{G}_{++}^{(e)}$ at fixed quasi-energy.

In the case where the Floquet-Bloch bands are non-degenerate, injective ($g_a(\nu) \neq g_a(\nu')$ for $\nu \neq \nu'$) and do not cross, each common eigenspace is one dimensional and the only possibility for redefining the Floquet-Bloch eigenstates is to introduce quasi-energy dependent phases:

$$|\psi_{a,\nu}\rangle \mapsto e^{i\theta_a(\nu)} |\psi_{a,\nu}\rangle. \quad (\text{C2})$$

Such quasi-energy dependent phases $\theta(\nu)$ fall into different topological sectors which are labeled by the winding number

$$n_w = \frac{1}{2\pi} \int_0^{2\pi f} \frac{d\theta(\nu)}{d\nu} d\nu. \quad (\text{C3})$$

For example $\theta_n(\nu) = nT\nu$ has winding number $n \in \mathbb{Z}$ and Eq. (16) implies that

$$\left| \varphi_{a,l}^{[e^{i\theta_n}]} \right\rangle = |\varphi_{a,l+n}\rangle. \quad (\text{C4})$$

Consequently, a topologically non-trivial phase has the same effect as combining a translation by an integer number of periods with a topologically trivial energy-dependent phase.

In the case of n degenerate Floquet-Bloch bands over the whole quasi-energy interval, the above phases are replaced by a quasi-energy dependent unitary transformation $U(\nu) \in \mathcal{U}(n)$ for $0 \leq \nu < 2\pi f$ so that, considering A_α the set of n band indexes, the new Wannier functions are defined by:

$$\left| \varphi_{a,l}^{[U]} \right\rangle = \frac{1}{\sqrt{f}} \int_0^{2\pi f} \sum_{b \in A_\alpha} U_{a,b}(\nu) |\psi_{b,\nu}\rangle \frac{d\nu}{2\pi}. \quad (\text{C5})$$

Such transformations are directly relevant when a source emits n single-electron excitations on top of the Fermi sea. In this case $g_a(\nu) = 1$ for several values of a . The topological sectors of such quasi-energy dependent unitaries are classified by the topological sectors of the overall phase since all groups $\text{SU}(n \geq 2)$ are simply connected. Let us now discuss in more detail the properties of the Floquet-Bloch band structure to see which situation is more likely to be encountered.

A first observation is that bands may have discontinuities. From our observations for classical voltage drives and for the mesoscopic capacitor driven by a sinusoidal or square voltage, it seems that such discontinuities appear when temperature is non-zero, for purely a.c. sources.

Finally, since physical states are defined up to a phase, we have an extra possibility for defining electronic atoms of signals in the case of flat bands. For example, one could replace Eq. (17) by its projective version, that is introducing a phase in front of $|\varphi_{a,l+1}\rangle$. Combining this with Eq. (C1) leads to

$$U_\Omega |\psi_{a,\nu}\rangle = |\psi_{a,\nu+\Omega}\rangle, \quad (\text{C6})$$

where the addition is considered modulo $2\pi f$ ($\Omega \in \mathbb{R}/2\pi f\mathbb{Z}$). Substituting this into Eq. (16) leads to

$$\left| \varphi_{a,l}^{[U_\Omega]} \right\rangle = e^{i\Omega T} |\varphi_{a,l+1}\rangle. \quad (\text{C7})$$

The time translation property (17) is satisfied up to a phase.

2. Minimal-spreading principle

Let us now discuss the general method used to determine suitable electronic atoms of signals. Exactly as in solid-state physics, a natural idea is to look for

maximally-localized Wannier functions [53]. Let us consider φ_a such a wave-function, the spreading $\langle (\Delta t)^2 \rangle_{\varphi_a}$ is defined as

$$\langle (\Delta t)^2 \rangle_{\varphi_a} = v_F \int_{\mathbb{R}} t^2 |\varphi_{a,0}(t)|^2 dt - \left(v_F \int_{\mathbb{R}} t |\varphi_{a,0}(t)|^2 dt \right)^2. \quad (\text{C8})$$

Let us consider directly the case of n degenerated bands $g_a(\nu) = p_a(\nu)$ for all $0 \leq \nu < 2\pi f$ and $a \in A_\alpha$. We then have a quasi-energy dependent unitary transformation ambiguity described by Eq. (C5). Maximally localized Wannier wavefunctions are now found by minimizing the quadratic functional

$$\mathcal{S}[U] = \sum_{a \in A_\alpha} \langle (\Delta t)^2 \rangle_{|\varphi_a^{[U]}\rangle} \quad (\text{C9})$$

over $U(\nu) \in \mathcal{U}(n)$ for $0 \leq \nu < 2\pi f$. Note that the right-hand side of Eq. (C8) may be divergent due to the large time behavior of $|\varphi_{a,0}(t)|^2$ as, for example, in the case of a Leviton train. In such a case, we should therefore regularize it by subtracting the same quantity for a reference choice of the unitary operator such as $U(\nu) = \mathbf{1}$.

Numerically, the implementation of the minimization process is straightforward in the case of a non-degenerate band. Since there is a natural cut-off for the length of the wavepacket, in this case it is easy to compute the functional (C8) from an arbitrary phase (C2). More importantly, it is also easy to compute the gradient, giving access to all efficient gradient-based minimization algorithms. In our case, we rely on the GSL implementation of the Fletcher-Reeves algorithm [94]. It consists in a succession of line minimizations. We begin at a given point (which can either be random phase or a null phase), and the first direction of minimization is given by the gradient. Then, at each iteration, a new direction is chosen, depending on the previous search direction, the gradient of current iteration and the norm of the gradient of previous iteration. The iteration ends when the gradient is orthogonal to the line of search.

For the degenerate case (C5), there are several difficulties. First, we need to parametrize the unitary matrices $U(\nu)$. For this, we introduce $\Theta(\nu)$, Hermitian matrices such that

$$U(\nu) = \exp(i\Theta(\nu)). \quad (\text{C10})$$

The main difficulty here is that, since $\mathcal{U}(n \leq 2)$ is a non-commutative group, it becomes hard to compute the gradients of the functional $\mathcal{S}[U]$. However, it is still easy to compute them if we consider a starting point at $U = \mathbf{1}$. In the following, we will denote $|\psi_{A,\nu}\rangle$ the vector containing every wavefunctions $|\psi_{a,\nu}\rangle$ with $a \in A$, A being the degenerate set of bands we want to minimize on. The matrix $U(\nu)$ acts on this vector space, mixing wavefunctions. At each iteration $n > 1$ of the algorithm, we now replace the wavefunctions $|\psi_{A,\nu}^{(n-1)}\rangle$ by the wavefunctions

$$\left| \psi_{A,\nu}^{(n)} \right\rangle = e^{ix_n H_n(\nu)} \left| \psi_{A,\nu}^{(n-1)} \right\rangle, \quad (\text{C11})$$

H_n being the search direction and x_n the real parameter that minimize this search direction. This allows us to always start the line minimization process from $U = \mathbb{1}$. To determine the minimum, we check whether our search direction is orthogonal to the local gradient computed by shifting $e^{ix_n H_n(\nu)}$ to identity. What makes everything work is that all quantities needed to compute the new direction of minimization are either invariant on the point of the $U(n)$ group we consider them (norm of the previous gradient), computed locally (the new gradient) or trivially transported (previous search direction, which is parallel to the transport). After N iterations, we end up with

$$\left| \psi_{A,\nu}^{(N)} \right\rangle = e^{i\Theta_N(\nu)} \dots e^{i\Theta_1(\nu)} \left| \psi_{A,\nu}^{(0)} \right\rangle. \quad (\text{C12})$$

emphasizing the non-commutative character of the group we are minimizing on.

Appendix D: HBT and HOM current noise

1. Explicit expressions

The outgoing current correlation $S_{11}^{(\text{out})}(t, t') = \langle i_{1\text{out}}(t) i_{1\text{out}}(t') \rangle - \langle i_{1\text{out}}(t) \rangle \langle i_{1\text{out}}(t') \rangle$ after a quantum point contact whose scattering matrix is

$$\begin{pmatrix} \sqrt{\mathcal{R}} & i\sqrt{\mathcal{T}} \\ i\sqrt{\mathcal{T}} & \sqrt{\mathcal{R}} \end{pmatrix}$$

has been computed in Ref. [43] in terms of the incoming current correlators and single electron coherences:

$$S_{11}^{(\text{out})}(t, t') = \mathcal{R}^2 S_{11}^{(\text{in})}(t, t') + \mathcal{T}^2 S_{22}^{(\text{in})}(t, t') + \mathcal{RT} \mathcal{Q}(t, t') \quad (\text{D1})$$

in which

$$\mathcal{Q}(t, t') = e^2 v_F^2 \left(\mathcal{G}_1^{(e)}(t', t) \mathcal{G}_2^{(h)}(t', t) + [1 \leftrightarrow 2] \right) \quad (\text{D2})$$

encodes two-particle interferences effects between the two incoming channels. The excess current noise is therefore given by

$$\Delta S_{11}^{(\text{out})}(t, t') = \mathcal{R}^2 \Delta S_{11}^{(\text{in})}(t, t') + \mathcal{T}^2 \Delta S_{22}^{(\text{in})}(t, t') \quad (\text{D3a})$$

$$+ \mathcal{RT} \Delta \mathcal{Q}(t, t'). \quad (\text{D3b})$$

Hanbury Brown and Twiss (HBT) experiments correspond to one of the sources being switched *on* and the other one being switched *off*. From now on, let us assume that both sources S_1 and S_2 are identical and synchronized. Under this hypothesis, $\Delta S_{11}^{(\text{in})} = \Delta S_{22}^{(\text{in})} = \Delta S_S$ is the excess noise generated by the source.

At zero temperature, the HBT excess zero frequency current noise can be expressed using the Floquet–Bloch spectrum as $\mathcal{RT} \Delta \mathcal{Q}_{\text{HBT}}$ where

$$\Delta \mathcal{Q}_{\text{HBT}} = e^2 \int_0^{2\pi f} \left[\sum_a g_a^{(e)}(\nu) + \sum_b g_b^{(h)}(\nu) \right] \frac{d\nu}{2\pi} \quad (\text{D4})$$

in which $\Delta \mathcal{Q}_{\text{HBT}}$ (see Eq. (D3b)) arises from the partitioning of electron and hole excitations at the QPC not contained in the partitioning of the incoming current noises (r.h.s of Eq. (D3a) at zero frequency). This leads to Eq. (29a).

When both sources are switched *on*, an Hong–Ou–Mandel experiment is performed. Using Eq. (D3), the corresponding excess noise is the sum of the excess noise of the two possible HBT experiments

$$\Delta S_{11}^{(\text{out})} = \Delta S_1^{(\text{HBT})} + \Delta S_2^{(\text{HBT})} + \mathcal{RT} \Delta \mathcal{Q}_{\text{HOM}} \quad (\text{D5})$$

and of a two-excitations interference contribution involving the two sources S_1 and S_2 which can be expressed as

$$\begin{aligned} \Delta \mathcal{Q}_{\text{HOM}} = & -2e^2 \int_0^{2\pi f} \left(\sum_a g_a^{(e)}(\nu)^2 + \sum_b g_b^{(h)}(\nu)^2 \right) \frac{d\nu}{2\pi} \\ & - 4e^2 \sum_{a,b} \int_0^{2\pi f} \left| g_{ab}^{(eh)}(\nu) \right|^2 \frac{d\nu}{2\pi} \end{aligned} \quad (\text{D6})$$

using the Floquet–Bloch analysis of the single electron coherence emitted by the source S_1 , identical to S_2 here. Adding twice the r.h.s. of Eq. (D4) (one for each source) to the r.h.s. of Eq. (D6) leads to the total contribution $(\mathcal{R}^2 + \mathcal{T}^2) \Delta S_S$ to the zero frequency current noise that comes on top of the partitioning of the sources intrinsic excess current noise ΔS_S . In the end, as shown on Fig. 17, the final expression (28c) for the excess zero frequency current noise at the HOM dip is the sum of the excess current noise of the sources transmitted by the two sources (which is always positive), to which is added the total two-excitation interference contribution given by Eq. (29b).

2. The HOM dip

Let us now use this to discuss the depth of the HOM dip defined as the difference between the HOM excess noise given by Eq. (D5) and the sum of the two HBT noises. Counting the dip’s depth positively, its expression is

$$[\Delta S_{\text{dip}}] = -\mathcal{RT} \Delta \mathcal{Q}_{\text{HOM}} \quad (\text{D7})$$

where $\Delta \mathcal{Q}_{\text{HOM}}$ is given by Eq. (D6).

It is interesting to rewrite these expressions in terms of physically more appealing quantities. For this, let us introduce an infrared regularization to compute traces of T -periodic operators. Let

$$\mathbf{X} = \sum_a \int_0^{2\pi f} X_a(\nu) \frac{d\nu}{2\pi} \quad (\text{D8})$$

a diagonal operator in the basis of electronic Floquet–Bloch eigenstates. The trace of this operator, which is defined and acts on \mathcal{H}_+ is divergent. Nevertheless, we

can regularize it. Inverting Eq. (16), its expression in the basis formed by the electronic atoms of signals is

$$\mathbf{X} = \sum_a \sum_{(l_+, l_-) \in \mathbb{Z}^2} X_a(l_+ - l_-) |\varphi_{a, l_+}\rangle \langle \varphi_{a, l_-}|. \quad (\text{D9})$$

in which $X_a(l)$ is related to $X_a(\nu)$ by Eq. (19). Taking the trace over a subspace generated by the electronic atoms of signal over a range of N periods gives

$$\text{Tr}_N(\mathbf{X}) = N \sum_a \int_0^{2\pi f} X_a(\nu) \frac{d\nu}{2\pi f}. \quad (\text{D10})$$

This leads to the definition of the per-period regularized trace as $\bar{X} = \text{Tr}_N(\mathbf{X})/N$. With this definition, the average number of electronic and hole excitations emitted per period are given by

$$\bar{N}_e = \sum_a \int_0^{2\pi f} g_a^{(e)}(\nu) \frac{d\nu}{2\pi f} \quad (\text{D11a})$$

$$\bar{N}_h = \sum_b \int_0^{2\pi f} g_b^{(h)}(\nu) \frac{d\nu}{2\pi f}. \quad (\text{D11b})$$

The quadratic terms in the eigenvalues or in the electron/hole coherences appearing in Eq. (D6) correspond to what would be obtained, assuming Wick's theorem be valid. Therefore, we denote these quantities with a “w” index. Using Wick's theorem with $\mathbf{G}^{(e)}$ as single electron coherence, the second moments of the numbers of excitations emitted per periods would be given by

$$(\Delta N_e)_w^2 = \sum_a \int_0^{2\pi f} g_a^{(e)}(\nu)(1 - g_a^{(e)}(\nu)) \frac{d\nu}{2\pi f} \quad (\text{D12a})$$

$$(\Delta N_h)_w^2 = \sum_b \int_0^{2\pi f} g_b^{(h)}(\nu)(1 - g_b^{(h)}(\nu)) \frac{d\nu}{2\pi f} \quad (\text{D12b})$$

$$\text{Cov}(N_e, N_h)_w = \sum_{a,b} \int_0^{2\pi f} |g_{ab}^{(eh)}(\nu)|^2 \frac{d\nu}{2\pi f}. \quad (\text{D12c})$$

Let us stress that, in the presence of interactions, these are not the actual moments of the numbers of electronic and hole excitations. The actual values differ from these Wick values by a contribution arising from the difference between the intrinsic excess second order coherence introduced in Ref. [28] and its expected value from Wick's theorem.

The absolute upper bound of the depth of the HOM dip is given by the HBT contribution $[\Delta S_{\text{dip}}^{(\text{max})}] = 2e^2 f \mathcal{R} \mathcal{T} \bar{N}_{\text{tot}}$ where $\bar{N}_{\text{tot}} = \bar{N}_e + \bar{N}_h$ represents to average total number of excitations emitted per period. Using the above notations, the difference between the maximum dip and the actual dip is then equal to

$$[\Delta S_{\text{dip}}^{(\text{max})}] - [\Delta S_{\text{dip}}] = 2e^2 f \mathcal{R} \mathcal{T} [(\Delta N_e)_w^2 + (\Delta N_h)_w^2 - 2 \text{Cov}(N_e, N_h)_w]. \quad (\text{D13a})$$

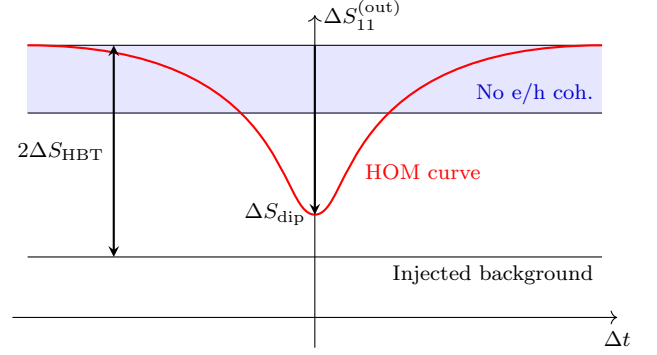


FIG. 17: Depth of the HOM dip at zero temperature: in an HOM experiment, the excess low frequency current noise is above the background noise ($\mathcal{R}^2 + \mathcal{T}^2$) ΔS_S injected by the sources. When the sources, which emit localized excitations, are sufficiently desynchronized, the current noise is expected to reach $\Delta S_{\text{HBT}} = e^2 f \mathcal{R} \mathcal{T} (\bar{N}_e + \bar{N}_h)$ exceeding this background noise by $2\Delta S_{\text{HBT}}$. At fixed Floquet–Bloch spectra ($g_a^{(e)}(\nu), g_b^{(h)}(\nu)$), the depth of the HOM dip has a lower bound which translates into an upper bound for the excess noise equal to $2e^2 f \mathcal{R} \mathcal{T} ((\Delta N_e)_w^2 + (\Delta N_h)_w^2)$ above the injected background noise (light blue zone). This bound is reached for vanishing electron/hole coherences.

The r.h.s is therefore directly proportional to the fluctuation $(\Delta Q)_w^2$ of the excess charge emitted per period by the source. In units of $-e$, the excess charge operator is given by

$$\hat{Q} = \int_{\mathbb{R}} : c^\dagger(\omega) c(\omega) : d\omega. \quad (\text{D14})$$

where the fermionic normal ordering is relative to the reference Fermi sea at chemical potential $\mu = 0$. Consequently, the ratio of the dip to its absolute upper bound is given by:

$$\frac{[\Delta S_{\text{dip}}]}{[\Delta S_{\text{dip}}^{(\text{max})}]} = 1 - \frac{(\Delta Q)_w^2}{\bar{N}_{\text{tot}}}. \quad (\text{D15})$$

If the many-body state does satisfy Wick's theorem, which is the case whenever interactions can be neglected, then having a maximally deep HOM dip corresponds to the actual vanishing charge fluctuations.

Appendix E: Many-body state and Floquet scattering theory

1. The Floquet-Bloch many-body state

In this appendix, we discuss the connexion between our approach and the T -periodic single-electron scattering theory that transforms the Fermi sea at chemical potential $\nu = 0$ into a pure many-body state. This corresponds to writing down the explicit form of the many-body op-

erator \mathcal{S} whose action corresponds to single-particle scattering

$$\psi_{\text{out}}(t) = \mathcal{S}\psi_{\text{in}}(t)\mathcal{S}^\dagger = \int S(t, t')\psi_{\text{in}}(t') dt \quad (\text{E1})$$

where $S(t, t')$ denotes the T -periodic single-particle scattering matrix in the time-domain representation. Without lack of generality, we shall consider here the case of an ac Floquet source, that is a single particle scattering operator \mathcal{S} leading to a vanishing average dc-current.

Finding an expression for \mathcal{S} is important for two reasons: first it gives insights on the action of Floquet sources on the incoming equilibrium state at the many-body level, then it enables us to connect the form of the many-body operator to the Floquet-Bloch spectrum and eigenstates and electron-hole coherences between them.

a. Two modes

Let us first discuss the simple two-mode case where only one electron mode φ_e and one hole mode φ_h are considered. At zero temperature, the incoming hole mode φ_h is filled and contains exactly one electron whereas the incoming electron mode φ_e is empty. The Floquet source will scatter the mode φ_h into a linear combination of φ_e and φ_h .

We will show that the operator \mathcal{S} can be written as

$$\mathcal{S} = \mathcal{S}_d \mathcal{S}_p \quad (\text{E2})$$

$$\mathcal{S}_d = \exp(\lambda \psi^\dagger[\varphi_e] \psi[\varphi_h] - \lambda^* \psi^\dagger[\varphi_h] \psi[\varphi_e]) \quad (\text{E3})$$

$$\mathcal{S}_p = \exp(i(\theta_e(\psi^\dagger \psi)[\varphi_e] + \theta_h(\psi^\dagger \psi)[\varphi_h])) \quad (\text{E4})$$

In this decomposition, \mathcal{S}_d is a displacement-like operator, with the complex parameter λ . It corresponds to the scattering processes of between the electron and hole modes. \mathcal{S}_p is a phase-shifting operator, that independently the phases of the incoming electron and hole modes. Since we can reabsorb the phase of λ by changing the relative phase between the wavefunctions φ_e and φ_h , we will consider $\lambda \in \mathbb{R}^+$.

Let us first focus on the displacement-like operator. The exponential can be expanded using the following identity

$$-(\psi^\dagger[\varphi_e] \psi[\varphi_h] - \psi^\dagger[\varphi_h] \psi[\varphi_e])^2 = n_e(1 - n_h) + n_h(1 - n_e) = \Pi_{\text{odd}}, \quad (\text{E5})$$

where $n_{e/h} = (\psi^\dagger \psi)[\varphi_{e/h}]$ denotes the number operator for the corresponding $\varphi_{e/h}$ mode and Π_{odd} is the projector on the one-particle sector. If we also introduce the orthogonal projector Π_{even} that projects on the zero or two-particle sector, a simple expression for the many-body scattering operator follows:

$$\mathcal{S}_d = \Pi_{\text{even}} + \Pi_{\text{odd}} [\cos \lambda + \sin \lambda (\psi^\dagger[\varphi_e] \psi[\varphi_h] - \psi^\dagger[\varphi_h] \psi[\varphi_e])]. \quad (\text{E6})$$

Applying the operator \mathcal{S} to the creation operators leads to

$$\begin{aligned} \mathcal{S}\psi^\dagger[\varphi_e]\mathcal{S} &= \cos \lambda e^{i\theta_e} \psi^\dagger[\varphi_e] - \sin \lambda e^{i\theta_h} \psi^\dagger[\varphi_h] \\ \mathcal{S}\psi^\dagger[\varphi_h]\mathcal{S} &= \cos \lambda e^{i\theta_h} \psi^\dagger[\varphi_h] + \sin \lambda e^{i\theta_e} \psi^\dagger[\varphi_e]. \end{aligned} \quad (\text{E7})$$

The outgoing creation operators are thus linear combinations of the incoming creation operators. The corresponding linear operator involved is indeed unitary and any unitary operator can be brought in that form by tuning the phase between the wavefunctions φ_e and φ_h .

b. The many-mode case

To understand the full many-body case, we first recast our Floquet-Bloch analysis in terms of the scattering operator. For this, we split the scattering operator into two parts. The first one rearranges electrons and holes independently and is described by a unitary matrix $e^{i(\Theta^{(h)} + \Theta^{(e)})}$, where $\Theta^{(h)}$ and $\Theta^{(e)}$ are Hermitian matrices acting on the hole and electron subspaces respectively. These operators generalize the phases θ_h and θ_e of the previously discussed two-mode example. Their action on the Fermi sea is, as we shall see, to add a global phase to the many-body state. The second part involves a two-mode scattering process, in which each pair of modes is scattered according such that

$$\begin{aligned} \mathcal{S}\psi^\dagger[\varphi_e]\mathcal{S} &= u\psi^\dagger[\varphi_e] + v\psi^\dagger[\varphi_h] \\ \mathcal{S}\psi^\dagger[\varphi_h]\mathcal{S} &= u\psi^\dagger[\varphi_h] - v\psi^\dagger[\varphi_e]. \end{aligned} \quad (\text{E8})$$

with $u, v \in \mathbb{R}_+$. The mathematical details for such a decomposition of general unitary operators can be found in Appendix E 2.

The final result of this procedure is an expression of the full many-body scattering operator as a product of uncoupled elementary two-mode operators, with a prefactor that scatters electron and hole subspaces independently:

$$S = \exp \left(\sum_{a \in \mathbb{N}} \int_0^{2\pi f} \lambda_a(\nu) \left(\psi^\dagger[\psi_{a,\nu}^{(e)}] \psi[\psi_{a,\nu}^{(h)}] - \psi^\dagger[\psi_{a,\nu}^{(h)}] \psi[\psi_{a,\nu}^{(e)}] \right) \frac{d\nu}{2\pi} \right) \quad (\text{E9a})$$

$$\times \exp \left(i \sum_{a,b \in \mathbb{N}} \int_0^{2\pi f} \left(\Theta_{ab}^{(e)}(\nu) \psi^\dagger[\psi_{a,\nu}^{(e)}] \psi[\psi_{b,\nu}^{(e)}] + \Theta_{ab}^{(h)}(\nu) \psi^\dagger[\psi_{a,\nu}^{(h)}] \psi[\psi_{b,\nu}^{(h)}] \right) \frac{d\nu}{2\pi} \right). \quad (\text{E9b})$$

Furthermore, when the bands are flat, we can reorganize a combination of Floquet-Bloch modes as a combination of electronic atoms of signals directly at the many-body level. Of course the choice of Floquet-Wannier functions in the electron quadrant will constrain the choice of Floquet-Wannier functions in the hole quadrant. Namely, we have

$$\int_0^{2\pi f} \psi^\dagger[\psi_{a,\nu}^{(e)}] \psi[\psi_{a,\nu}^{(h)}] \frac{d\nu}{2\pi} = \sum_{l \in \mathbb{Z}} \psi^\dagger[\varphi_{a,l}^{(e)}] \psi[\varphi_{a,l}^{(h)}]. \quad (\text{E10})$$

2. Splitting unitary matrices

In this appendix, we will introduce a decomposition for unitary matrices useful when we partition equally the Hilbert space in two. In what remains, we will consider a matrix $S \in \text{U}(2n)$, acting on a Hilbert space $\mathcal{H} = \mathcal{H}_+ \otimes \mathcal{H}_-$, where $\dim \mathcal{H}_+ = \dim \mathcal{H}_- = n$. The goal here is to show that there exists an orthogonal change of basis $P = P_- P_+$ that acts independently on \mathcal{H}_+ and \mathcal{H}_- in which we can write

$$PSP^\dagger = \left(\begin{array}{c|c} u & v \\ \hline v & -u \end{array} \right) e^{i(\Theta_- + \Theta_+)} \quad (\text{E11})$$

where $u, v \in \mathcal{M}_n$ are positive real diagonal matrices, Θ_\pm are Hermitian matrices of size n . The first block-column corresponds to the Hilbert space \mathcal{H}_- and the second one corresponds to \mathcal{H}_+ .

Generically, one can write the S matrix as

$$S = \left(\begin{array}{c|c} S_{--} & S_{-+} \\ \hline S_{+-} & S_{++} \end{array} \right). \quad (\text{E12})$$

For the sake of simplicity, we will consider that each submatrix is invertible. Other cases would correspond to either fully scattered modes or fully reflected modes, which can be separated from the start without much problems.

We will first introduce the polar decomposition of $S_{--} = H_{--} e^{i\theta_-}$, where θ_- is Hermitian and H_{--} is a positive semi-definite Hermitian matrix. This allows us to rewrite S as

$$S = \left(\begin{array}{c|c} H_{--} & S_{-+} \\ \hline S_{+-} e^{-i\theta_-} & S_{++} \end{array} \right) e^{i\theta_-}. \quad (\text{E13})$$

H_{--} being positive semi-definite, we can write it as $H_{--} = P_-^\dagger u P_-$, where u is a diagonal, real-valued, positive matrix. This leads us to

$$P_- S P_-^\dagger = \left(\begin{array}{c|c} u & S'_{-+} \\ \hline S'_{+-} & S_{++} \end{array} \right) e^{i\Theta_-}. \quad (\text{E14})$$

where $\Theta_- = P_- \theta_- P_-^\dagger$, $S'_{+-} = P_- S_{+-} e^{-i\theta_-}$ and $S'_{-+} = S_{-+} P_-^\dagger$. The first matrix of the rhs must be unitary. Since u is diagonal, it imposes that each column of S'_{+-} is orthogonal to each other. As such, we can rewrite this matrix as a product of a unitary matrix and a diagonal positive real matrix, $S'_{+-} = P_+^\dagger v$. Noting $P = P_- P_+$, we have shown

$$PSP^\dagger = \left(\begin{array}{c|c} u & S''_{-+} \\ \hline v & S'_{++} \end{array} \right) e^{i\Theta_-}. \quad (\text{E15})$$

where $S''_{-+} = S'_{-+} P_+^\dagger$, $S'_{++} = P_+ S_{++} P_+^\dagger$.

We can now use the hermitian properties of unitary matrices to build explicitly the constraints between u , v , S'_{++} and S''_{-+} . The orthogonality constraint gives us

$$S'_{++} = -(u/v) S''_{-+} \quad (\text{E16})$$

where u/v is the diagonal matrix formed by uv^{-1} . Conversely, the normalization conditions give us

$$S'_{++}^\dagger (\mathbb{1}_n + (u/v)^2) S'_{++} = \mathbb{1} \quad (\text{E17})$$

Since $u^2 + v^2 = \mathbb{1}$, this shows that $v^{-1} S'_{++} = e^{i\Theta_+}$, where Θ_+ is an Hermitian matrix. Putting everything together, we have

$$PSP^\dagger = \left(\begin{array}{c|c} u & v \\ \hline v & -u \end{array} \right) e^{i(\Theta_- + \Theta_+)}. \quad (\text{E18})$$

This is the property we wanted to show.

3. Many-body state at non-zero temperature

At non-zero temperature, all terms of Eq. (E9) will play a role. The contribution Eq. (E9b), arising from the separate rearrangement of electron and hole modes will have a non-trivial contribution to the total state. This

contribution may scatter electrons deep into the Fermi sea compared to the thermal scale into the thermal fluctuations. It will as well scatter holes from the thermal fluctuations deeper into the Fermi sea. It is also possible to rearrange wavefunctions inside the thermal band. Similar processes appear in the electron subspace. Notably, this term will explicitly couple different bands. The contribution Eq. (E9a) will also act differently, since sectors of even parities are expected if one of the Floquet-Bloch waves possesses thermal fluctuations at this point. We expect that the atoms of signal, as well as their respective coherences to be modified by this term.

Remarkably, the description in terms of Floquet-Bloch waves at zero temperature allows us to give a many-body description up to the two Hermitian operators $\Theta^{(e)}$ and $\Theta^{(h)}$. This is interesting since it gives a way to see which processes will occur when “heating” an ideal single-electron source. Our approach may thus lead to new insights on the effect of non-zero temperatures on electronic correlations studied in Refs. [84, 85].

Appendix F: The purity indicator

Wick’s theorem is valid whenever the many-body state ρ of the electron fluid is Gaussian

$$\rho = \frac{e^{-\psi^\dagger \cdot \mathbf{K} \cdot \psi}}{Z_{\mathbf{K}}} \quad (\text{F1})$$

where $Z_{\mathbf{K}} = \text{Tr}(e^{-\psi^\dagger \cdot \mathbf{K} \cdot \psi})$ is the corresponding partition function. The \mathbf{K} operator is related to the single-electron

coherence through

$$\mathbf{G}^{(e)} = (\mathbf{1} + e^{\mathbf{K}})^{-1} \quad (\text{F2})$$

The many-body “unregularized” purity indicator $\mathbb{P}_\rho^{(\text{un})} = \text{Tr}(\rho^2)$ can then formally rewritten as a quotient on infinite dimensional determinants over the single-particle space of states \mathcal{H}_{1p} . Using Eq. (F2), it can then be conveniently expressed in terms of the total single-electron coherence:

$$\mathbb{P}_\rho^{(\text{un})} = \frac{\text{Det}[\mathbf{1} + e^{2\mathbf{K}}]}{\text{Det}[\mathbf{1} + e^{\mathbf{K}}]^2} \quad (\text{F3a})$$

$$= \text{Det}[\mathbf{1} + 2((\mathbf{G}^{(e)})^2 - \mathbf{G}^{(e)})] \quad (\text{F3b})$$

We can now use the decomposition of the total single-electron coherence $\mathbf{G}^{(e)} = \mathbf{\Pi}_h + \Delta_0 \mathbf{G}^{(e)}$ where $\mathbf{\Pi}_h$ denotes the projection onto the space of hole excitations and

$$\Delta_0 \mathbf{G}^{(e)} = \begin{pmatrix} \mathbf{g}_e & \mathbf{g}_{eh} \\ \mathbf{g}_{he} & -\mathbf{g}_h \end{pmatrix} \quad (\text{F4})$$

is the excess single-electron coherence with respect to the Fermi sea to obtain an expression for the purity indicator only in terms of data that can be reconstructed by the single-electron tomography protocol. These are \mathbf{g}_e , \mathbf{g}_h and the off diagonal parts \mathbf{g}_{eh} and \mathbf{g}_{he} . This finally leads to:

$$\mathbb{P}_\rho^{(\text{un})} = \left| \begin{array}{cc} \mathbf{1} - 2[\mathbf{g}_e(\mathbf{1} - \mathbf{g}_e) - \mathbf{g}_{eh}\mathbf{g}_{he}] & 2[\mathbf{g}_{eh}\mathbf{g}_h - \mathbf{g}_e\mathbf{g}_{eh}] \\ 2[\mathbf{g}_h\mathbf{g}_{he} - \mathbf{g}_{he}\mathbf{g}_e] & \mathbf{1} - 2[\mathbf{g}_h(\mathbf{1} - \mathbf{g}_h) - \mathbf{g}_{he}\mathbf{g}_{eh}] \end{array} \right| \quad (\text{F5})$$

The final step involves using the fact that, for a T -periodic sources, all these operators are block diagonal with respect to the decomposition of the single-particle state into subspaces indexed by the quasi-energy $\nu \in [0, 2\pi f]$. Let us consider a block diagonal 1-particle operator \mathbf{M} block-diagonal with respect to the quasi-energy ν . Its determinant can be approximated by discretizing the first Floquet-Brillouin zone $[0, 2\pi f]$:

$$\ln \left[\prod_{n=0}^{N-1} \text{Det} \left(\mathbf{M}_{\frac{2\pi n f}{N}} \right) \right] \simeq N \int_0^{2\pi f} \text{Tr}(\ln(\mathbf{M}_\nu)) \frac{d\nu}{2\pi f} \quad (\text{F6})$$

in which \mathbf{M}_ν precisely denotes the restriction of \mathbf{M} to the subspace of single-particle state with quasi-energy ν . Such a discretization corresponds to juxtaposing N periods of duration T and considering states with periodic boundary conditions on this interval, thereby introducing a formal IR regularization.

This finally gives us the following compact expression for the many-body purity indicator:

$$\mathbb{P}_\rho = \exp \left[\int_0^{2\pi f} \ln (1 - 2A(\nu)(1 - A(\nu)) - 2B(\nu)(1 - B(\nu))) \frac{d\nu}{2\pi f} \right] \quad (\text{F7})$$

in which

$$A(\nu) = g^{(ee)}(\nu)(1 - g^{(hh)}(\nu)) - |g^{(eh)}(\nu)|^2 \quad (\text{F8})$$

$$B(\nu) = g^{(hh)}(\nu)(1 - g^{(ee)}(\nu)) - |g^{(eh)}(\nu)|^2 \quad (\text{F9})$$

are computed in terms of the eigenvalues $g^{(ee)}(\nu)$ and $g^{(hh)}(\nu)$ obtained from our diagonalization algorithm (see Section III) and of the corresponding electron/hole coherences $g^{(eh)}(\nu)$. Discussion of the conditions for unit purity can be found in Ref. [9]: it corresponds to a pure many-body state of the form

$$|\Psi\rangle = \prod_{0 \leq \nu < 2\pi f} \left(u(\nu) + v(\nu)\psi^\dagger[\varphi_\nu^{(e)}]\psi[\varphi_\nu^{(h)}] \right) |F\rangle \quad (\text{F10})$$

where $|u(\nu)|^2 + |v(\nu)|^2 = 1$ for all $0 \leq \nu < 2\pi f$.

Appendix G: Mesoscopic capacitor: case of a square drive

In the case of a square drive used to demonstrate single-electron emission by the mesoscopic capacitor [1], the T -periodic voltage drive is defined by $V_g(t) = -V/2$ for $-T/2 \leq t < 0$ and $V_g(t) = V/2$ for $0 < t < T/2$.

1. Electron/hole entanglement

Figure 18 presents a density plot of the entropy defined by Eq. (43) as a function of D and eV/Δ at fixed $\Delta/hf = 20$. There are shallow zones with minima in each square $eV/\Delta \in [n, n+1]$ ($n \in \mathbb{N}$) and $0 < D \leq 1$. In the single-electron sector, a global minimum can be found at $eV_{\text{opt}}/\Delta \approx 0.37$ and $D_{\text{opt}} \approx 0.47$ and the corresponding entropy is 0.20 bit. As we shall see, this is the regime where the mesoscopic capacitor behaves almost ideally, emitting exactly one electron and one hole excitation per period.

There is also a minimum in the second square where $1 < eV/\Delta \leq 2$ but the zone is further from zero. In this zone, three electrons are emitted during the first half period and three holes during the other one, due to the fact that at zero voltage, there is a level at the Fermi energy. It is not surprising that in this zone the deviation from the ideal regime is greater than in the previous case, since we expect a generation of more electron/hole pairs.

A surprising feature are the substructures that appear within each shallow zone. At the time of this writing, we do not yet understand this fact. Further numerical

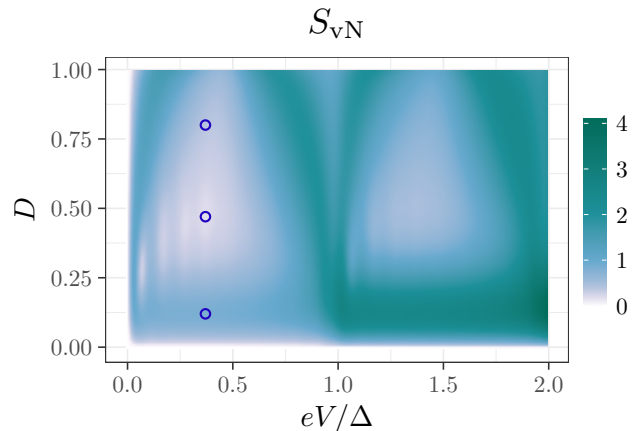


FIG. 18: Density plot of the electron/hole entanglement entropy at zero temperature for the mesoscopic capacitor operated with a square drive of frequency f such that $\Delta/hf = 20$ as a function of eV/Δ and D .

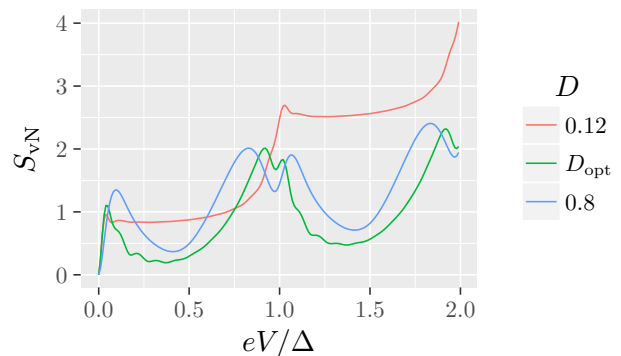


FIG. 19: Cuts of the entropy S_{vN} for a square voltage drive depicted on Fig. 18 as functions of eV/Δ for $D = 0.12$, $D = D_{\text{opt}}$ and $D = 0.8$.

exploration will be necessary, especially to see if the ratio Δ/hf plays a role in these substructures.

In order to understand more precisely the electron/hole entanglement properties described by this plot, we have chosen specific points for which we will push the analysis further. The corresponding electronic Wigner distribution functions are plotted on Fig. 20.

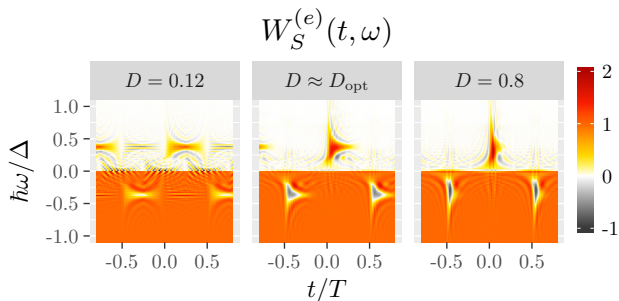


FIG. 20: Density plot of the full Wigner distribution function $W_S^{(e)}(t, \omega)$ for the square-voltage driven mesoscopic capacitor as a function of t/T and $\hbar\omega/\Delta$ for the three selected points appearing on Fig. 18.

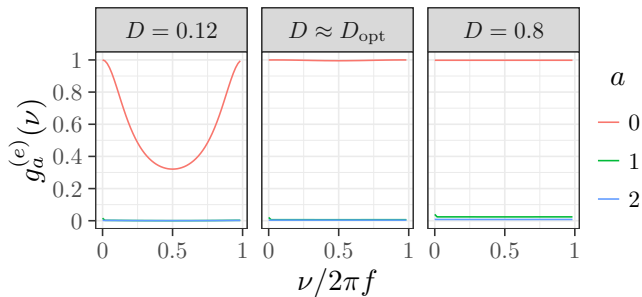


FIG. 21: Floquet-Bloch spectrum for the three selected points appearing on Fig. 18, in the case of a square-voltage mesoscopic capacitor. Only the first three bands are represented, all the other ones being even closer to zero.

2. The Floquet-Bloch spectrum

Let us review the Floquet-Bloch spectrum for the three points that are marked in Fig. 18. This figure presents the corresponding bands as functions of the adimensionned quasi-energy $\omega/2\pi f$ and orders them according to their averages, the $a = 0$ band being one with the highest average.

The middle panel corresponds to the absolute minimum of the entropy and therefore to the best operating point as a single-electron source. Only one band gives eigenvalues close to one and it is flat. All the other bands are really close to zero as expected.

Opening the dot ($D = 0.8$, right panel) leads to flat bands as expected since at $D = 1$ it is really what is expected but we note that the eigenvalues are almost unity and that the $a = 1$ band has value 0.02, thus showing that we are departing from the ideal single-electron regime.

Closing the dot ($D = 0.12$, left panel) mostly changes the shape of the $a = 0$ band which shows some curvature. Its average is equal to 0.57 which shows that strong electron/hole coherences are expected.

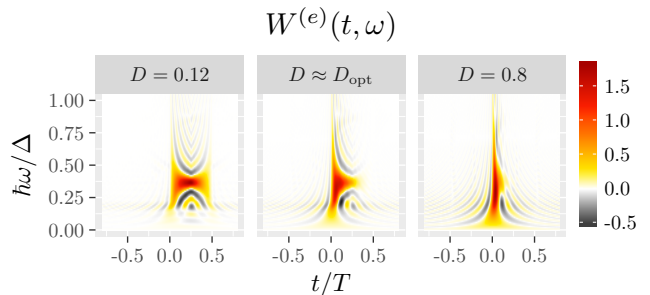


FIG. 22: Wigner distribution functions for the Floquet-Wannier electronic atoms of signal corresponding to the $a = 0$ Floquet-Bloch band represented as a function of t/T and $\hbar\omega/\Delta$ for the three operating points of Fig. 18 in the case of a square voltage drive.

3. Electronic atoms of signals and coherences

In order to get a clearer view of the electronic state emitted by the source, let us now extract the corresponding electronic atoms of signal. Figure 22 presents the electronic atoms of signal associated with the $a = 0$ Floquet-Bloch band for the three operating points considered before.

As expected, the duration of each wavepacket increases with decreasing D reflecting the fact that the escaping time from the dot is longer at low QPC transparency. At the optimal value D_{opt} , we expect the source to emit a wavepacket of the form

$$\tilde{\varphi}_e(\omega) = \frac{\mathcal{N}_e H(\omega)}{\omega - \omega_e - i\gamma_e/2}, \quad (\text{G1})$$

where \mathcal{N}_e ensures normalization and γ_e denotes the electron escape rate from the quantum dot which is given by $\gamma_e = D\Delta/h(1 - D/2)$ [46, 95]. We note that for $D = 0.12$, the electronic wavepacket remains limited to the first half period $0 \lesssim t \lesssim T/2$. At very low D , we expect this wavepacket to be the projection on the space of single-particle states with positive energy of the dual of the Martin-Landauer wavepacket, that is of an electronic wavefunction constant on a time interval.

Since the bands are flat for $D = D_{opt}$ and $D = 0.8$, no inter-period coherence is expected as can be seen from the middle and right panels of Fig. 23. However, when closing the dot ($D \approx 0.12$, left panel), inter-period coherences for the electronic excitations start to unfold, an expected consequence of the delocalization of the emitted electronic excitations over more than a half period. This shows that the electronic coherence time is given by the electronic escape time which, in this case, exceeds the duration of an electronic atom of signal.

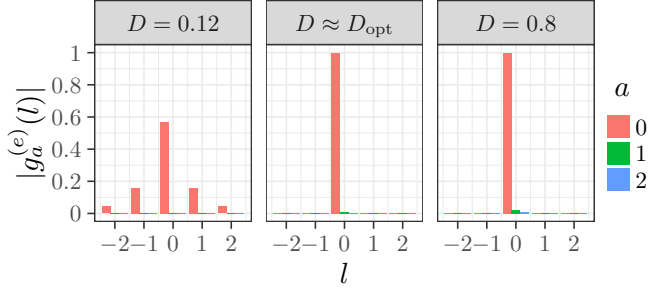


FIG. 23: Temporal coherences $p_n(\Delta l)$ between the electronic atoms of signal of the $a = 0, 1$ and 2 Floquet-Bloch bands given by Eq. (19) as a function of Δl for the three operating points of Fig. 18 in the case of a square drive.

Appendix H: Wavefunctions within a Leviton train

We define a Levitonoid as a normalized wavefunction $\psi(t)$ such that their time translations by multiples of T are mutually orthogonal and $\sum_{l \in \mathbb{Z}} \psi(t - lT) \psi^*(t' - lT)$ is the excess electronic first-order coherence generated by a T -periodic train of Lorentzian pulses. As we will see, this wavefunction is not unique but, in the case of a T -periodic Leviton train, analytical expressions for the minimally-spread Levitonoids can be obtained.

1. The Moskalets atoms of signal

In a recent work [47], Moskalets has identified one possible Levitonoid as:

$$\psi(t) = \sqrt{\frac{\tau_0}{\pi}} \frac{1}{t - i\tau_0} \prod_{n=1}^{\infty} \frac{t + nT + i\tau_0}{t + nT - i\tau_0} \quad (\text{H1})$$

where $T = 1/f$ is the period and τ_0 is the typical time width of the excitation. This wavefunction has a spatial extension given by τ_0 .

To discuss its energy content, let us use the identity

$$\Gamma(z) = \frac{1}{z} \prod_{n=1}^{\infty} \frac{(1 + \frac{1}{n})^z}{1 + \frac{z}{n}} \quad (\text{H2})$$

to rewrite the infinite product as a ratio of Γ functions, up to a global phase

$$\frac{\Gamma((t - i\tau_0)/T)}{\Gamma((t + i\tau_0)/T)} = \frac{t + i\tau_0}{t - i\tau_0} \prod_{n=1}^{\infty} \left(1 + \frac{1}{n}\right)^{-2i\tau_0} \quad (\text{H3a})$$

$$\prod_{n=1}^{\infty} \frac{t + nT + i\tau_0}{t + nT - i\tau_0} \quad (\text{H3b})$$

Then, up to a global phase factor, we can rewrite:

$$\psi(t) = \sqrt{\frac{\tau_0}{\pi}} \frac{1}{t + i\tau_0} \frac{\Gamma((t - i\tau_0)/T)}{\Gamma((t + i\tau_0)/T)}. \quad (\text{H4})$$

Fourier transforming this wavepacket gives, up to global phase factor:

$$\psi(\omega) = \frac{1}{\sqrt{\mathcal{N}}} \text{H}(\omega) \left(2 \sin \frac{\nu T}{2}\right)^{2i\tau_0/T} e^{-\omega_{\text{int}} \tau_0} \quad (\text{H5})$$

where $\omega = \omega_{\text{int}} + \nu$, with $\nu \in [0, 2\pi f]$ and thus $\omega_{\text{int}} = 2\pi f \lfloor \omega / 2\pi f \rfloor$. Here, $\mathcal{N} = f/v_F(1 - e^{-4\pi\tau_0/T})$ is a normalization factor and H the Heaviside step function. We can then rewrite the wavefunction as a real part and a periodic phase:

$$\psi(\omega) = \frac{1}{\sqrt{\mathcal{N}}} \text{H}(\omega) e^{i\theta(\omega)} e^{-\omega_{\text{int}} \tau_0} \quad (\text{H6})$$

with the phase satisfying the condition $\theta(\omega + 2\pi f) = \theta(\omega)$. This expression shows that the electronic distribution function of this Levitonoid is the staircase approximation of an exponential decay, with step widths given by $2\pi f$ as expected from T -periodicity. Note that the electronic distribution function does not depend on the phase $\theta(\omega)$.

2. The minimally-spread atoms of signal

The Moskalets Levitonoids having a spreading τ_0 , they are naturally expected to be among the minimally-spread atoms of signals when $f\tau_0 \ll 1$, that is when the Leviton spacing is large compared to their duration. But in the opposite limit $f\tau_0 \gtrsim 1$, this is certainly not the case. Let us search for other Levitonoids that could be spread over the period T and clarify the relation between our algorithm and Moskalets work [47].

If a quantum electrical current has a time-reversal symmetry, which is the case for a Leviton train, then there must be a set of Wannier wavefunctions that possess this symmetry. Consequently, there is a set of real valued Wannier functions in the frequency domain: $\varphi_{\text{Lev}}(\omega) \in \mathbb{R}$. Assuming that $\varphi_{\text{Lev}}(\omega) \geq 0$, the time-spreading minimization problem becomes trivial and we find that, up to time-translation by T , the minimal wavefunctions are the ones that possess the time-reversal symmetry.

In the case of Levitonoids, Eq. (H6) shows that the wavefunctions can be written as the product of a real part and a phase part, the phase part being periodic in time. Thus the minimization of Eq. (C8) is realized when the minimal wavefunction has a constant phase. Setting this global phase to zero, we have the following wavefunction:

$$\varphi_{\text{Lev}}(\omega) = \frac{1}{\sqrt{\mathcal{N}}} \text{H}(\omega) e^{-\omega_{\text{int}} \tau_0} \quad (\text{H7})$$

which is time-reversal invariant. In this case, the current of one pulse is different from the current of one Leviton of duration τ_0 . The time-domain expression for this wavepacket is:

$$\varphi_{\text{Lev}}(t) = \frac{i}{\sqrt{\mathcal{N}'} } \frac{1}{t} \frac{1 - e^{-2i\pi f t}}{1 - e^{-2\pi f(\tau_0 + it)}} \quad (\text{H8})$$

The corresponding average current $i_{\text{Lev}}(t) = -v_F |\varphi(t)|^2$ (in units of $-e$) is then

$$i_{\text{Lev}}(t) \propto \frac{\text{sinc}^2(\pi f t)}{1 - \cos(2\pi f t) / \cosh(2\pi f \tau_0)}. \quad (\text{H9})$$

The overlap between this wavepacket and a unique Leviton φ_1 is given by

$$|\langle \varphi_{\text{Lev}} | \varphi_1 \rangle|^2 = \frac{1}{\pi f \tau_0} \frac{1 - e^{-2\pi f \tau_0}}{1 + e^{-2\pi f \tau_0}}. \quad (\text{H10})$$

The behavior when $f\tau_0 \ll 1$ is approached by

$$|\langle \varphi_{\text{Lev}} | \varphi_1 \rangle|^2 \simeq 1 - \frac{(\pi f \tau_0)^2}{6} \quad (\text{H11})$$

making the Leviton approximation a fairly good approximation in this case. When $f\tau_0 \gg 1$, we have a rather slow decay:

$$|\langle \varphi_{\text{Lev}} | \varphi_1 \rangle|^2 \simeq \frac{1}{\pi f \tau_0}. \quad (\text{H12})$$

3. Obtention from Martin-Landauer's wavepackets

As noticed in [67, Appendix 5], at zero temperature, the effect of a T -eriodic classical drive V_d is to reshuffle the Martin-Landauer wavepackets associated with a given period through a unitary transformation of the following form:

$$|\text{ML}_{n,l}\rangle \mapsto \sum_{k \in \mathbb{Z}} p_k[V_d] |\text{ML}_{n+k,l}\rangle \quad (\text{H13})$$

in which $|\text{ML}_{n,l}\rangle$ denotes the time translated to period l of the single-particle state defined by Eq. (24) and $p_k[V_d]$ is the photoassisted transition amplitude associated with this drive. In the case of a Leviton train, the photoassisted amplitudes p_k are known and given by [67]

$$p_{k < -1} = 0 \quad (\text{H14a})$$

$$p_{-1} = e^{-2\pi f \tau_0} \quad (\text{H14b})$$

$$p_{k \geq 0} = (1 - e^{-4\pi f \tau_0}) e^{-2\pi k f \tau_0} \quad (\text{H14c})$$

Consequently, introducing $\beta = e^{-2\pi f \tau_0}$ for compacity, for all states with the Fermi sea ($n \leq -1$):

$$|\text{ML}_{-n,l}\rangle \mapsto -\beta |\text{ML}_{-(n+1),l}\rangle + (1 - \beta^2) \sum_{k=1}^n \beta^{n-k} |\text{ML}_{-k,l}\rangle \quad (\text{H15a})$$

$$+ (1 - \beta^2) \beta^n \sum_{q=0}^{+\infty} \beta^q |\text{ML}_{q,l}\rangle \quad (\text{H15b})$$

in which we have separated what remains into the Fermi sea (first line) from what emerges from the Fermi sea (second line). This shows that, as expected, the projection

of the single-particle scattering from the space generated by the Martin-Landauer wavepackets of negative energy and given period onto the space of state generated by the ones of positive energy is of rank 1. This is sufficient to obtain an electronic atom of signal for the Leviton associated with the period l is

$$|\text{Lev}_l\rangle = \sqrt{1 - \beta^2} \sum_{p=0}^{+\infty} \beta^p |\text{ML}_{p,l}\rangle. \quad (\text{H16})$$

Since the Martin-Landauer wavepacket $\text{ML}_{n,l=0}$ has a non-zero constant wavefunction over $2\pi n f \leq \omega < 2\pi(n+1)f$ and zero for $\omega \geq 2\pi(n+1)f$ or $\omega < 2\pi n f$, the wavefunction of $|\text{Lev}_1\rangle$ in the frequency domain is exactly given by Eq. (H7) therefore showing that it is indeed the minimally-spread Levitonoid!

Appendix I: Random emission

1. Expression in the frequency domain

Let us start from the excess coherence of a random train of $-e$ charge Lorentzian pulse

$$\Delta \mathcal{G}^{(e)}(t + \tau/2, t - \tau/2) = \mathcal{G}_F^{(e)}(\tau) \frac{\cos(2\pi\theta_p(f\tau)) - \cos(2\pi f(\tau/2 - i\tau_0))}{\cos(2\pi f(\tau/2 - i\tau_0)) - \cos(2\pi f t)}. \quad (\text{I1})$$

This expression is periodic in t with a period $T = 1/f$. The n -th harmonics $A_n(\tau)$ of its Fourier series expansion is then given by

$$A_n(\tau) = -i \mathcal{G}_F(\tau) \frac{\cos(2\pi\theta_p(f\tau)) - \cos(2\pi f(\tau/2 - i\tau_0))}{\sin(2\pi f(\tau/2 - i\tau_0))} \times e^{-2\pi|n|f\tau_0} e^{-i\pi|n|f\tau}. \quad (\text{I2})$$

Performing the Fourier transform along the variable τ leads to the energy representation of the first-order coherence. Let us notice that the Fourier transform is found to be zero when $\omega < \pi|n|$, meaning that the first-order coherence is non-zero only in the electronic quadrant, as expected. By looking at the electronic quadrant, we derive

$$\mathcal{G}_{+,n}^{(e)}(\omega) = \text{H}(\omega - \pi f|n|) e^{-2\omega\tau_0} \mathcal{F}_p(\omega + \pi n f) \quad (\text{I3})$$

where $\mathcal{F}_p(\omega)$ is a $2\pi f$ -periodic real-valued function defined by the sum

$$\mathcal{F}_p(\omega) = \frac{i}{\pi} \sum_{k \in \mathbb{Z}} \frac{\cos(\chi_p(k)) - 1}{k + 2if\tau_0} e^{i\omega k T} \quad (\text{I4})$$

where $\chi_p(x) = 2\pi\theta_p(2if\tau_0 + k) - \pi k$. In order to evaluate numerically this expression, we will decompose $\mathcal{F}_p = \mathcal{F}_p^{(\text{sing})} + \mathcal{F}_p^{(\text{reg})}$, where $\mathcal{F}_p^{(\text{sing})}$ contains singularities

due to the slow decay ($\sim 1/k$) at infinity. We have

$$\mathcal{F}_p^{(\text{sing})}(\omega) = \frac{i}{\pi} \sum_{k \in \mathbb{Z}} \frac{\cosh(4\pi p \tau_0) - 1}{k + 2if\tau_0} e^{i\omega k T} \quad (\text{I5})$$

$$\mathcal{F}_p^{(\text{reg})}(\omega) = \frac{i}{\pi} \sum_{k \in \mathbb{Z}} \frac{\cos(\chi_p(k)) - \cosh(4\pi p \tau_0)}{k + 2if\tau_0} e^{i\omega k T}. \quad (\text{I6})$$

The singular part then contributes to the single-electron coherence by

$$\mathcal{G}_{+,n}^{(e,\text{sing})}(\omega) = 4 \text{H}(\omega - \pi f|n|) \frac{\sinh^2(2\pi f p \tau_0)}{e^{4\pi f \tau_0} - 1} e^{-2\omega_n \tau_0} \quad (\text{I7})$$

where $\omega_n = 2\pi f \lfloor \omega/2\pi f \rfloor$ if n is even and $\omega_n = 2\pi f \lfloor \omega/2\pi f - 1/2 \rfloor + \pi f$ if n is odd. The regular part can then be evaluated numerically by direct summation. To be more precise, we can bound the truncation error on the regular part, when using K terms on the sum. Using an asymptotic expansion, we find that the error scales as

$$\epsilon = 16p(1-p)(f\tau_0)^2 \frac{\sinh(4\pi p f \tau_0)}{K}. \quad (\text{I8})$$

On top of the polynomial scaling, we notice an exponential scaling in p and in $f\tau_0$. Actually, as we will see later, we can use a symmetry in $p \leftrightarrow 1-p$, to ensure that all the computations are done at $p \leq 1/2$. With that, it is reasonable to compute the sum for $\tau \lesssim 1$.

When $p = 1$, the regular contribution cancels out, and we find the usual expression for a Leviton train. When $p \rightarrow 0$, it is the singular contribution that disappears first (scaling as p^2) leaving only the regular contribution (scaling as p). When $p \ll \min(1, f\tau_0)$, $\mathcal{F}_p(\omega) = 4\pi f p \tau_0$ is constant. Each harmonics of the first-order coherence is thus an exponential decay

$$\mathcal{G}_{+,n}^{(e)}(\omega) = 4\pi f p \text{H}(\omega - \pi|n|f) \tau_0 e^{-2\omega \tau_0}. \quad (\text{I9})$$

2. Electronic atoms of signal

The electronic atoms of signal describing the random train's first order coherence are obtained by following the method presented in Section III. The projection of the single-electron coherence on the electronic quadrant has non-zero matrix elements only for $\omega_{\pm} = \nu + 2\pi n_{\pm} f$ in which $0 \leq \nu < 2\pi f$ and n_{\pm} are positive integers. This corresponds to $\omega = (\omega_+ + \omega_-)/2 = \nu + \pi f(n_+ + n_-)$ and $\Omega = \omega_+ - \omega_- = 2\pi(n_+ - n_-)f$. Then, using Eq. (I3) and the periodicity of $\mathcal{F}_p(\Omega)$ in $\Omega \rightarrow \Omega + 2\pi f$, the excess first order electronic coherence can be rewritten as

$$\Delta_0 \mathbf{G}^{(e)} = \int_0^{2\pi f} e^{-2\nu \tau_0} \mathcal{F}_p(\nu) \mathbf{M}(\nu) \frac{d\nu}{2\pi f} \quad (\text{I10a})$$

$$\mathbf{M}(\nu) = \sum_{n_{\pm} \in \mathbb{N}} e^{-2\pi(n_+ + n_-)f\tau_0} |\nu + 2\pi f n_+ \rangle \langle \nu + 2\pi f n_- | \quad (\text{I10b})$$

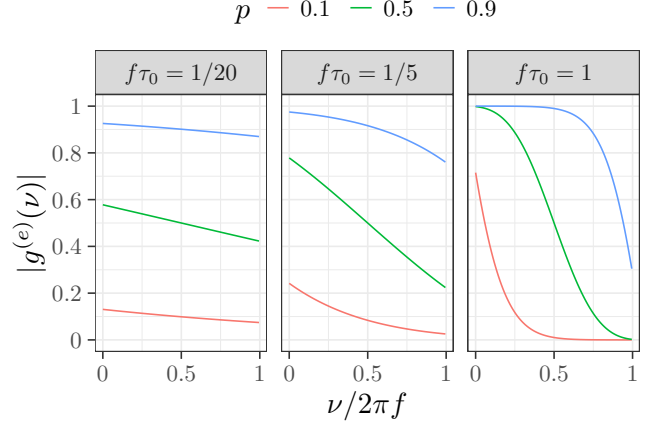


FIG. 24: Floquet-Bloch spectrum for the random train of Lorentzian pulses (it has only one band) for width $f\tau_0 = 1/10, 1/5$ and 1 for three different values of p ($1/10, 1/2$ and $9/10$). Bands are more and more flat when decreasing $f\tau_0$ as expected since, in this limit, one recovers the random emission of a single electronic atom of signal per period with probability p . When p goes to unity, we see the band getting closer to a flat band at value one, which corresponds to the T -periodic train of Levitons.

We thus have to diagonalize the operator $\mathbf{M}(\nu)$ for each $0 \leq \nu < 2\pi f$. We have already seen how to diagonalize it: for each ν , this operator has rank one and its eigenvector is the one obtained in Eq. (H16). This immediately shows that we have the same Floquet-Bloch states (only one band here) and therefore the same electronic atoms of signals than for the periodic Leviton train ($p = 1$, Appendices H2 and H3).

Only the eigenvalue is modified by randomness:

$$g^{(e)}(\nu) = (1 - e^{-4\pi f \tau_0})^{-1} e^{-2\nu \tau_0} \mathcal{F}_p(\nu). \quad (\text{I11})$$

When $p = 1$, the periodic Leviton train with its flat band with $g^{(e)}(\nu = 1)$ is recovered but for $p < 1$, the band is not flat anymore. This means that for $p < 1$, the emission probability of emission of the Levitonoid is lower than unity but this also leads to inter-period coherences between the Levitonoids. A numerical evaluation of the r/h/s of Eq. (I11) is shown on Fig. 24 which confirms these features.

Finally, using this last expression, we can rewrite the zeroth-harmonic of the first order coherence as

$$\mathcal{G}_0^{(e)}(\omega) = (1 - e^{-4\pi f \tau_0}) e^{-2\pi f \lfloor \frac{\omega}{2\pi f} \rfloor \tau_0} g^{(e)}(\omega). \quad (\text{I12})$$

By performing the inverse Fourier transform on this expression, we can thus express the coherences between the time-shifted Levitonoids as $g^{(e)}(l) = T A_0(-lT)$. Thus, we find

$$g^{(e)}(l = 0) = p \quad (\text{I13})$$

$$g^{(e)}(l \neq 0) = \frac{i}{2\pi l} \frac{\cosh(2\pi f \tau_0) - (-1)^l \cos(2\pi \theta_p(-l))}{\sinh 2\pi f \tau_0} \quad (\text{I14})$$

This expression satisfies $g_p^{(e)}(l \neq 0) = -g_{1-p}^{(e)}(l)^*$ which leads to the symmetry property

$$g_p^{(e)}(\omega) = 1 - g_{1-p}^{(e)}(-\omega). \quad (\text{I15})$$

We use this symmetry to perform all the numerical computations at $p \leq 1/2$.

3. Resumming inter-period coherences

In Appendix I2, we have seen that it was possible to decompose the signal on Levitonoids. In a sense, Levitonoids are proper atoms of signals, because they do not overlap when they are time-shifted by an integer number of periods. However, when $p < 1$, coherences appear between time-shifted Levitonoids.

Remarkably, is it possible to express the excess single-electron coherence $\mathbf{G}_{R_p}^{(e)}$ in terms of wavefunctions associated with each period (and obtained by applying the translation operator \mathbf{T}_T), each of them emitted with probability p , without any inter-period coherence:

$$\Delta_0 \mathbf{G}^{(e)} = p \sum_{l \in \mathbb{Z}} |\text{Gla}_{p,l}\rangle \langle \text{Gla}_{p,l}| \quad (\text{I16})$$

in which $|\text{Gla}_{p,l}\rangle = \mathbf{T}_T^l |\text{Gla}_p\rangle$ is obtained by a time translation by l periods from

$$|\text{Gla}_p\rangle = \int_0^{+\infty} \sqrt{\frac{1 - e^{-4\pi f \tau_0}}{p f}} e^{-\omega_{\text{int}} \tau_0} \sqrt{g^{(e)}(\omega)} |\omega\rangle d\omega \quad (\text{I17})$$

in which $\omega_{\text{int}} = 2\pi f [\omega/2\pi f]$. We will call such a single-particle state a p -Glattlion in reference to [42]. However, the overlap of adjacent p -Glattlions is non-vanishing and is related to the electronic coherences between two different periods in the minimally-spread Levitonoids:

$$p \langle \text{Gla}_{p,0} | \text{Gla}_{p,l} \rangle = \int_0^{2\pi f} g^{(e)}(\nu) e^{i\nu l T} \frac{d\nu}{2\pi f} = g^{(e)}(l) \quad (\text{I18})$$

In other words, the coherences between the Levitonoids are given by the overlap between time-shifted p -Glattlions which, therefore, cannot be considered as electronic atoms of signals. Despite this non vanishing overlap, it is quite remarkable that the excess single-electron coherence for the random train of Levitons can be rewritten in such a simple form.

Finally, it's worth noting that the 1-Glattlion is nothing else than the minimal Levitonoid. On the other hand, when $p \rightarrow 0$, a p -Glattlion becomes close to isolated Levitons. This is related to the fact that when p is small, pulses are emitted as if they were isolated: the probability for a single pulse to be separated by a distance at least k from the previous and the next one is $(1-p)^{2k}$ which goes to unity when $p \rightarrow 0$. As such, they do not exhibit Pauli exclusion principle between pulses.

-
- [1] G. Fève, A. Mahé, J. Berroir, T. Kontos, B. Plaças, D. Glattli, A. Cavanna, B. Etienne, and Y. Jin, *Science* **316**, 1169 (2007).
- [2] C. Leicht, P. Mirovsky, B. Kaestner, F. Hols, V. Kashcheyevs, E. Kurganova, U. Zeitler, T. Weimann, K. Pierz, and H. Schumacher, *Semicond. Sci. Technol.* **26**, 055010 (2011).
- [3] J. Dubois, T. Jullien, C. Grenier, P. Degiovanni, P. Roulleau, and D. C. Glattli, *Phys. Rev. B* **88**, 085301 (2013), URL <http://link.aps.org/doi/10.1103/PhysRevB.88.085301>.
- [4] M. Kataoka, N. Johnson, C. Emary, P. See, J. P. Griffiths, G. A. C. Jones, I. Farrer, D. A. Ritchie, M. Pepper, and T. J. B. M. Janssen, *Phys. Rev. Lett.* **116**, 126803 (2016), URL <https://link.aps.org/doi/10.1103/PhysRevLett.116.126803>.
- [5] J. D. Fletcher, P. See, H. Howe, M. Pepper, S. P. Giblin, J. P. Griffiths, G. A. C. Jones, I. Farrer, D. A. Ritchie, T. J. B. M. Janssen, et al., *Phys. Rev. Lett.* **111**, 216807 (2013), URL <http://link.aps.org/doi/10.1103/PhysRevLett.111.216807>.
- [6] S. Hermelin, S. Takada, M. Yamamoto, S. Tarucha, A. Wieck, L. Saminadayar, C. Bäerle, and T. Meunier, *Nature* **477**, 435 (2011).
- [7] J. Gabelli and B. Reulet, *Phys. Rev. B* **87**, 075403 (2013).
- [8] E. Bocquillon, V. Freulon, F. Parmentier, J. Berroir, B. Plaças, C. Wahl, J. Rech, T. Jonckheere, T. Martin, C. Grenier, et al., *Ann. Phys. (Berlin)* **526**, 1 (2014).
- [9] R. Bisognin, A. Marguerite, B. Roussel, M. Kumar, C. Cabart, C. Chapdelaine, A. Mohammad-Djafari, J. M. Berroir, E. Bocquillon, B. Plaças, et al., *Nature Communications* **10**, 3379 (2019).
- [10] A. Bertoni, P. Bordone, R. Brunetti, C. Jacoboni, and S. Reggiani, *Phys. Rev. Lett.* **84**, 5912 (2000), URL <http://link.aps.org/doi/10.1103/PhysRevLett.84.5912>.
- [11] R. Ionicioiu, G. Amaratunga, and F. Udreă, *Int. J. Mod. Phys. B* **15**, 125 (2001).
- [12] A. Bertoni, *J. Comput. Electron.* **6**, 67 (2007).
- [13] T. Zibold, P. Vogl, and A. Bertoni, *Phys. Rev. B* **76**, 195301 (2007).
- [14] A. Bertoni, *Charge-Based Solid-State Flying Qubits* (Springer New York, New York, NY, 2009), pp. 1011–1027, ISBN 978-0-387-30440-3, URL https://doi.org/10.1007/978-0-387-30440-3_67.
- [15] M. Yamamoto, S. Takada, C. Bäerle, K. Watanabe, A. D. Wieck, and S. Tarucha, *Nature Nanotechnology* **7**, 247 (2012).

- [16] B. Bertrand, S. Hermelin, S. Takada, M. Yamamoto, S. Tarucha, A. Ludwig, A. D. Wieck, C. Bäuerle, and T. Meunier, *Nature Nanotechnology* **11**, 672 (2016), URL <https://doi.org/10.1038/nnano.2016.82>.
- [17] H. Flentje, P. A. Mortemousque, R. Thalineau, A. Ludwig, A. D. Wieck, C. Bäuerle, and T. Meunier, *Nature Communications* **8**, 501 (2017), URL <https://doi.org/10.1038/s41467-017-00534-3>.
- [18] C. W. J. Beenakker, D. P. DiVincenzo, C. Emary, and M. Kindermann, *Phys. Rev. Lett.* **93**, 020501 (2004).
- [19] C. H. W. Barnes, J. M. Shilton, and A. M. Robinson, *Phys. Rev. B* **62**, 8410 (2000), URL <https://link.aps.org/doi/10.1103/PhysRevB.62.8410>.
- [20] S. Takada, H. Edlbauer, H. V. Lepage, J. Wang, P.-A. Mortemousque, G. Georgiou, C. H. W. Barnes, C. J. B. Ford, M. Yuan, P. V. Santos, et al., *Nature Communications* **10**, 4557 (2019), URL <https://doi.org/10.1038/s41467-019-12514-w>.
- [21] R. Glauber, *Phys. Rev.* **130**, 2529 (1963).
- [22] G. C. Wick, A. S. Wightman, and E. P. Wigner, *Phys. Rev.* **88**, 101 (1952), URL <https://link.aps.org/doi/10.1103/PhysRev.88.101>.
- [23] N. Friis, *New Journal of Physics* **18**, 033014 (2016), URL <http://stacks.iop.org/1367-2630/18/i=3/a=033014>.
- [24] M. Johansson (2016), arXiv:1610.00539.
- [25] C. Grenier, R. Hervé, G. Fève, and P. Degiovanni, *Mod. Phys. Lett. B* **25**, 1053 (2011), proceedings of the Statphys 24 satellite meeting "International Conference on Frustrated Spin Systems, Cold Atoms and Nanomaterials" (Hanoi, 14-16 July 2010).
- [26] G. Haack, M. Moskalets, and M. Büttiker, *Phys. Rev. B* **87**, 201302(R) (2013).
- [27] M. Moskalets, *Phys. Rev. B* **89**, 045402 (2014), URL <http://link.aps.org/doi/10.1103/PhysRevB.89.045402>.
- [28] E. Thibierge, D. Ferraro, B. Roussel, C. Cabart, A. Marguerite, G. Fève, and P. Degiovanni, *Phys. Rev. B* **93**, 081302(R) (2016).
- [29] B. Roussel, C. Cabart, G. Fève, E. Thibierge, and P. Degiovanni, *Physica Status Solidi B* **254**, 16000621 (2017).
- [30] G. Haack, M. Moskalets, J. Splettstoesser, and M. Büttiker, *Phys. Rev. B* **84**, 081303(R) (2011), URL <http://link.aps.org/doi/10.1103/PhysRevB.84.081303>.
- [31] S. Ol'khovskaya, J. Splettstoesser, M. Moskalets, and M. Büttiker, *Phys. Rev. Lett.* **101**, 166802 (2008).
- [32] J. Splettstoesser, M. Moskalets, and M. Büttiker, *Phys. Rev. Lett.* **103**, 076804 (2009).
- [33] E. Bocquillon, V. Freulon, J. Berroir, P. Degiovanni, B. Plaçais, A. Cavanna, Y. Jin, and G. Fève, *Science* **339**, 1054 (2013).
- [34] T. Jullien, P. Roulleau, B. Roche, A. Cavanna, Y. Jin, and D. C. Glattli, *Nature* **514**, 603 (2014).
- [35] J. D. Fletcher, N. Johnson, E. Locane, P. See, J. P. Griffiths, I. Farrer, D. A. Ritchie, P. W. Brouwer, V. Kashcheyevs, and M. Kataoka, *Nature Communications* **10**, 5298 (2019), URL <https://doi.org/10.1038/s41467-019-13222-1>.
- [36] F. Bloch, *Zeitschrift für Physik* **52**, 555 (1929).
- [37] G. Wannier, *Physical Review* **52**, 191 (1937).
- [38] T. Martin and R. Landauer, *Phys. Rev. B* **45**, 1742 (1992).
- [39] F. Hassler, M. V. Suslov, G. M. Graf, M. V. Lebedev, G. B. Lesovik, and G. Blatter, *Phys. Rev. B* **78**, 165330 (2008).
- [40] J. Moura, *IEEE Signal Processing Magazine* **26**, 6 (2009).
- [41] Y. Yin, *J. Phys.: Condens. Matter* **31**, 245301 (2019).
- [42] D. C. Glattli and P. Roulleau, *Phys. Rev. B* **97**, 125407 (2018).
- [43] C. Grenier, R. Hervé, E. Bocquillon, F. Parmentier, B. Plaçais, J. Berroir, G. Fève, and P. Degiovanni, *New Journal of Physics* **13**, 093007 (2011).
- [44] R. Bisognin, H. Bartolomei, M. Kumar, I. Safi, J.-M. Berroir, E. Bocquillon, B. Plaçais, A. Cavanna, Y. Gennser, Y. Jin, et al., *Nature Communications* **10**, 1708 (2019).
- [45] D. Ferraro, A. Feller, A. Ghibaudo, E. Thibierge, E. Bocquillon, G. Fève, C. Grenier, and P. Degiovanni, *Phys. Rev. B* **88**, 205303 (2013).
- [46] A. Mahé, F. Parmentier, G. Fève, J. Berroir, T. Kontos, A. Cavanna, B. Etienne, Y. Jin, D. Glattli, and B. Plaçais, *Journal of Low Temperature Physics* **153**, 339 (2008).
- [47] M. Moskalets, *Phys. Rev. B* **91**, 195431 (2015), URL <http://link.aps.org/doi/10.1103/PhysRevB.91.195431>.
- [48] C. Wahl, J. Rech, T. Jonckheere, and T. Martin, *Phys. Rev. Lett.* **112**, 046802 (2014).
- [49] D. Ferraro, B. Roussel, C. Cabart, E. Thibierge, G. Fève, C. Grenier, and P. Degiovanni, *Phys. Rev. Lett.* **113**, 166403 (2014), URL <http://link.aps.org/doi/10.1103/PhysRevLett.113.166403>.
- [50] A. Marguerite, C. Cabart, C. Wahl, B. Roussel, V. Freulon, D. Ferraro, C. Grenier, J. M. Berroir, B. Plaçais, T. Jonckheere, et al., *Phys. Rev. B* **94**, 115311 (2016).
- [51] C. Cabart, B. Roussel, G. Fève, and P. Degiovanni, *Phys. Rev. B* **98**, 155302 (2018).
- [52] G. Floquet, *Ann. Ecole Norm. Sup.* **12**, 47 (1883).
- [53] N. Marzari, A. A. Mostofi, J. R. Yates, I. Souza, and D. Vanderbilt, *Rev. Mod. Phys.* **84**, 1419 (2012), URL <http://link.aps.org/doi/10.1103/RevModPhys.84.1419>.
- [54] E. Locane, P. W. Brouwer, and V. Kashcheyevs, *New Journal of Physics* **21**, 093042 (2019).
- [55] G. Yamahata, S. Ryu, N. Johnson, H. S. Sim, A. Fujiwara, and M. Kataoka, *Nature Nanotechnology* **14**, 1019 (2019), URL <https://doi.org/10.1038/s41565-019-0563-2>.
- [56] T. Wenz, F. Hohls, X. Jehl, M. Sanquer, S. Barraud, J. Knoch, G. Barinova, and V. Kashcheyevs, *Applied Physics Letters* **108**, 213107 (2016), URL <https://doi.org/10.1063/1.4951679>.
- [57] C. Altimiras, H. le Sueur, U. Gennser, A. Cavanna, D. Mailly, and F. Pierre, *Nature Physics* **6**, 34 (2010).
- [58] X. K. Yue and Y. Yin, *Phys. Rev. B* **99**, 235431 (2019), URL <https://link.aps.org/doi/10.1103/PhysRevB.99.235431>.
- [59] M. Vanević, Y. V. Nazarov, and W. Belzig, *Phys. Rev. B* **78**, 245308 (2008), URL <http://link.aps.org/doi/10.1103/PhysRevB.78.245308>.
- [60] M. Vanević, J. Gabelli, W. Belzig, and B. Reulet, *Phys. Rev. B* **93**, 041416(R) (2016), URL <http://link.aps.org/doi/10.1103/PhysRevB.93.041416>.
- [61] M. Vanevic, Y. V. Nazarov, and W. Belzig, *Physica Status Solidi B* **254**, 1600551 (2017).
- [62] L. Amico, R. Fazio, A. Osterloh, and V. Vedral, *Rev. Mod. Phys.* **80**, 517 (2008), URL <http://link.aps.org/>

- doi/10.1103/RevModPhys.80.517.
- [63] C. H. Bennett, H. J. Bernstein, S. Popescu, and B. Schumacher, Phys. Rev. A **53**, 2046 (1996), URL <https://link.aps.org/doi/10.1103/PhysRevA.53.2046>.
- [64] H. Li and F. D. M. Haldane, Phys. Rev. Lett. **101**, 010504 (2008).
- [65] H. F. Song, S. Rachel, C. Flindt, I. Klich, N. Laflorencie, and K. Le Hur, Phys. Rev. B **85**, 035409 (2012), URL <https://link.aps.org/doi/10.1103/PhysRevB.85.035409>.
- [66] I. Klich, J. Phys. A **39**, L85 (2006).
- [67] J. Dubois, T. Jullien, F. Portier, P. Roche, A. Cavanna, Y. Jin, W. Wegscheider, P. Roulleau, and D. Glatli, Nature **502**, 659 (2013).
- [68] L. Levitov, H. Lee, and G. Lesovik, J. Math. Phys. **37**, 4845 (1996).
- [69] M. Moskalets, *Scattering matrix approach to non-stationary quantum transport* (Imperial College Press, London, 2011).
- [70] M. Moskalets, P. Samuelsson, and M. Büttiker, Phys. Rev. Lett. **100**, 086601 (2008).
- [71] A. Marguerite, E. Bocquillon, J.-M. Berroir, B. Plaçais, P. Degiovanni, and G. Fève, Physica Status Solidi B **254**, 1600618 (2017).
- [72] M. Misiorny, G. Fève, and J. Splettstoesser, Phys. Rev. B **97**, 075426 (2018), URL <https://link.aps.org/doi/10.1103/PhysRevB.97.075426>.
- [73] C. Grenier, J. Dubois, T. Jullien, P. Roulleau, D. C. Glatli, and P. Degiovanni, Phys. Rev. B **88**, 085302 (2013), URL <http://link.aps.org/doi/10.1103/PhysRevB.88.085302>.
- [74] A. Papoulis, *Signal Analysis* (Mac-Graww Hill, 1977).
- [75] D. W. Bliss and K. W. Forsythe, in *The Thrity-Seventh Asilomar Conference on Signals, Systems Computers, 2003* (2003), vol. 1, p. 54.
- [76] G. Raleigh and J. Cioffi, IEEE Transactions on Communications **46**, 357 (1998).
- [77] V. Freulon, A. Marguerite, J. Berroir, B. Plaçais, A. Cavanna, Y. Jin, and G. Fève, Nature Communications **6**, 6854 (2015).
- [78] M. Moskalets, Phys. Rev. B **97**, 155411 (2018), URL <https://link.aps.org/doi/10.1103/PhysRevB.97.155411>.
- [79] R. Rodriguez, F. Parmentier, D. Ferraro, P. Roulleau, U. Gensser, A. Cavanna, M. Sassetti, F. Portier, D. Mailly, and P. Roche, Nature Communications **11**, 2426 (2020).
- [80] J. Romero, R. Babbush, J. R. McClean, C. Hempel, P. J. Love, and A. Aspuru-Guzik, Quantum Science and Technology **4**, 014008 (2018), URL <https://doi.org/10.1088%2F2058-9565%2Faad3e4>.
- [81] D. Dasenbrook and C. Flindt, Phys. Rev. B **92**, 161412 (2015), URL <https://link.aps.org/doi/10.1103/PhysRevB.92.161412>.
- [82] P. Hofer, D. Dasenbrook, and C. Flindt, Physica Status Solidi (b) **254**, 1600582 (2017).
- [83] D. Dasenbrook, J. Bowles, J. B. Brask, P. P. Hofer, C. Flindt, and N. Brunner, New Journal of Physics **18**, 043036 (2016), URL <http://stacks.iop.org/1367-2630/18/i=4/a=043036>.
- [84] M. Moskalets, Phys. Rev. B **96**, 165423 (2017).
- [85] M. Moskalets, Phys. Rev. B **98**, 115421 (2018).
- [86] D. Ferraro, C. Wahl, J. Rech, T. Jonckheere, and T. Martin, Phys. Rev. B **89**, 075407 (2014), URL <http://link.aps.org/doi/10.1103/PhysRevB.89.075407>.
- [87] D. Ferraro, T. Jonckheere, J. Rech, and T. Martin, Physica Status Solidi (b) **254**, 1600531 (2017), ISSN 1521-3951, 1600531, URL <http://dx.doi.org/10.1002/pssb.201600531>.
- [88] F. Ronetti, L. Vannucci, D. Ferraro, T. Jonckheere, J. Rech, T. Martin, and M. Sassetti, Phys. Rev. B **98**, 075401 (2018).
- [89] G. Gasse, C. Lupien, and B. Reulet, Phys. Rev. Lett. **111**, 136601 (2013).
- [90] J. C. Forgues, C. Lupien, and B. Reulet, Phys. Rev. Lett. **113**, 043602 (2014).
- [91] A. L. Grimsmo, F. Qassemi, B. Reulet, and A. Blais, Phys. Rev. Lett. **116**, 043602 (2016), arXiv:1507.00322.
- [92] S. Virally, J. O. Simoneau, C. Lupien, and B. Reulet, Phys. Rev. A **93**, 043813 (2016), URL <http://link.aps.org/doi/10.1103/PhysRevA.93.043813>.
- [93] D. Ferraro, F. Ronetti, J. Rech, T. Jonckheere, M. Sassetti, and T. Martin, Phys. Rev. B **97**, 155135 (2018), URL <https://link.aps.org/doi/10.1103/PhysRevB.97.155135>.
- [94] R. Fletcher and C. Reeves, Comput. J. **7**, 149 (1964).
- [95] S. E. Nigg and M. Büttiker, Phys. Rev. B **77**, 085312 (2008).
- [96] More precisely, $\mathcal{V}_d(t) = \int_{-\infty}^x (\partial_x U)(x, t - x/v_F) dx$ in which $U(x, t) = V_d(t)u(x)$ denotes the voltage seen by the electrons as they fly across the QPC ($u(x)$ being non zero close to the constriction of the QPC and rapidly vanishing away from it).